AD-A119 755 AIR FORCE INST OF TECH WRIGHT-PATTERSON AFB OH F/G 4/2
DIAGNOSTICS OF THE HEAT SOURCES AND SINKS OF THE ASIATIC MONSOO--ETC(U)
1981 D R JOHNSON, R D TOWNSEND
UNCLASSIFIED AFIT/CI/NR-81-35T NL

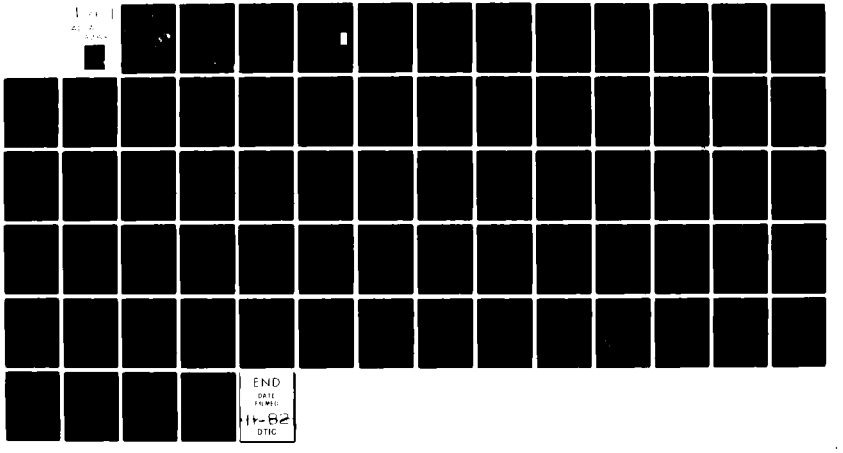

END
DATE FILMED
11-82
DTIC

UNCLASS

SECURITY CLASSIFICATION OF THIS PAGE (When Data Entered)

REPORT DOCUMENTATION PAGE	READ INSTRUCTIONS BEFORE COMPLETING FORM
1. REPORT NUMBER AFIT/CI/NR-81-35T	2. GOVT ACCESSION NO. AD-A119755	3. RECIPIENT'S CATALOG NUMBER
4. TITLE (and Subtitle) Diagnostics of the Heat Sources and Sinks of the Asiatic Monsoon and the Thermally-Forced Planetary Scale Response	5. TYPE OF REPORT & PERIOD COVERED THESIS/DISSERTATION
	6. PERFORMING ORG. REPORT NUMBER
7. AUTHOR(s) Donald R. Johnson and Ronald D. Towsend	8. CONTRACT OR GRANT NUMBER(s)
9. PERFORMING ORGANIZATION NAME AND ADDRESS AFIT STUDENT AT: Univ of Wisconsin-Madison	10. PROGRAM ELEMENT, PROJECT, TASK AREA & WORK UNIT NUMBERS
11. CONTROLLING OFFICE NAME AND ADDRESS AFIT/NR WPAFB OH 45433	12. REPORT DATE ? 1981
	13. NUMBER OF PAGES 47
14. MONITORING AGENCY NAME & ADDRESS(if different from Controlling Office)	15. SECURITY CLASS. (of this report) UNCLASS
	15a. DECLASSIFICATION/DOWNGRADING SCHEDULE
16. DISTRIBUTION STATEMENT (of this Report) APPROVED FOR PUBLIC RELEASE; DISTRIBUTION UNLIMITED	
17. DISTRIBUTION STATEMENT (of the abstract entered in Block 20, if different from Report)	
18. SUPPLEMENTARY NOTES APPROVED FOR PUBLIC RELEASE: IAW AFR 190-17 AIR FORCE INSTITUTE OF TECHNOLOGY (ATC) WRIGHT-PATTERSON AFB, OH 45433	LYNN E. WOLAVER Dean for Research and Professional Development 22 SEP 1982
19. KEY WORDS (Continue on reverse side if necessary and identify by block number)	
20. ABSTRACT (Continue on reverse side if necessary and identify by block number) ATTACHED	

DD FORM 1 JAN 73 1473 EDITION OF 1 NOV 65 IS OBSOLETE

UNCLASS

SECURITY CLASSIFICATION OF THIS PAGE (When Data Entered)

ABSTRACT

The purpose of this paper is to provide a descriptive analysis of the planetary scale isentropic mass circulation and energy transport forced by the global distribution of differential heating and to establish a link between mass circulation, energy transport and boundary processes in the satisfaction of global energy balance. Some insight into the global distribution of heating will be provided from the patterns of mass and energy transport, although at the time of preparation of this paper, explicit computations of the diabatic heating have not been completed. In the earlier work of Zillman (1972) and Otto (1974), planetary scale mass circulations associated with the irrotational mode of mass transport were determined from the climatological distribution of diabatic heating. While the fields of the irrotational mode in their work and ours are similar, a detailed comparative discussion of quantitative results has not been included due to the time constraint for completion of this paper for the Bergen Conference.

81-35T

AFIT RESEARCH ASSESSMENT

The purpose of this questionnaire is to ascertain the value and/or contribution of research accomplished by students or faculty of the Air Force Institute of Technology (ATC). It would be greatly appreciated if you would complete the following questionnaire and return it to:

AFIT/NR
Wright-Patterson AFB OH 45433

RESEARCH TITLE: Diagnostics of the Heat Sources and Sinks of the Asiatic Monsoon and the Thermally-Forced Planetary Scale Response

AUTHOR: Donald R. Johnson and Ronald D. Towsend

RESEARCH ASSESSMENT QUESTIONS:

1. Did this research contribute to a current Air Force project?

( ) a. YES ( ) b. NO

2. Do you believe this research topic is significant enough that it would have been researched (or contracted) by your organization or another agency if AFIT had not?

( ) a. YES ( ) b. NO

3. The benefits of AFIT research can often be expressed by the equivalent value that your agency achieved/received by virtue of AFIT performing the research. Can you estimate what this research would have cost if it had been accomplished under contract or if it had been done in-house in terms of manpower and/or dollars?

( ) a. MAN-YEARS _____ ( ) b. $_____

4. Often it is not possible to attach equivalent dollar values to research, although the results of the research may, in fact, be important. Whether or not you were able to establish an equivalent value for this research (3. above), what is your estimate of its significance?

( ) a. HIGHLY SIGNIFICANT ( ) b. SIGNIFICANT ( ) c. SLIGHTLY SIGNIFICANT ( ) d. OF NO SIGNIFICANCE

5. AFIT welcomes any further comments you may have on the above questions, or any additional details concerning the current application, future potential, or other value of this research. Please use the bottom part of this questionnaire for your statement(s).

NAME GRADE POSITION

ORGANIZATION LOCATION

STATEMENT(s):

FOLD DOWN ON OUTSIDE - SEAL WITH TAPE

AFIT/NR
WRIGHT-PATTERSON AFB OH 45433

OFFICIAL BUSINESS
PENALTY FOR PRIVATE USE, $300

NO POSTAGE
NECESSARY
IF MAILED
IN THE
UNITED STATES

BUSINESS REPLY MAIL
FIRST CLASS PERMIT NO. 73236 WASHINGTON D.C.

POSTAGE WILL BE PAID BY ADDRESSEE

AFIT/ DAA
Wright-Patterson AFB OH 45433

1

FOLD IN

81-35T

DIAGNOSTICS OF THE HEAT SOURCES AND SINKS OF THE ASIATIC MONSOON AND THE THERMALLY-FORCED PLANETARY SCALE RESPONSE

By Donald R. Johnson and Ronald D. Townsend
University of Wisconsin-Madison

Introduction

Fifty years ago Sir Napier Shaw (1942) discussed the planetary scale of mass exchange within an isentropic structure of the atmosphere and pointed towards the concept of thermally-forced planetary scale circulations. After dividing the atmosphere into an overworld of warmer air spanning the entire meridional extent of the atmosphere and an underworld of colder air restricted to higher latitudes, he emphasized that the overworld exchanged properties with the underworld through convection associated with diabatic processes. No exchange would be realized through adiabatic motion through which the geometric forms of the isentropic surfaces evolved. In the isentropic analysis of the planetary scale mass and energy transport from a FGGE (First GARP Global Experiment) data set presented herein, results that isolate the thermally-forced planetary scale circulations and the diabatic convective exchange through isentropic surfaces suggested by Sir Napier Shaw are now discussed.

The condition that planetary-scale mass circulations must exist is inferred from the isentropic equation of continuity. Horizontal mass transport from a heat source to a heat sink must occur in upper isentropic layers while the mass transport must be from heat sink to heat source in lower layers in order to satisfy the continuity requirements that mass transport is upward through isentropic surfaces in the heat source region and downward in

the heat sink region. These mass circulations must also serve to transport energy and momentum.

In the preliminary results from the FGGE data set presented herein, mass and energy transport by planetary scale circulations that directly link high and low latitudes is isolated. The results verify the early analyses of the planetary scale mass transport conducted by Zillman (1972) for the Southern Hemisphere and by Otto (1974) for the Northern Hemisphere. In these studies the planetary circulations and quasi-horizontal transport of mass and energy were inferred from the climatological distribution of heating. The counterpart presented herein infers the planetary circulations and large scale heating distribution from an analysis of the observed mass and energy transport. Previous attempts to infer the large scale heating distribution from observed data have been limited. Some of the earlier efforts were by Clapp (1961) and Wiin-Nielsen and Brown (1962), in association with attempts to estimate the generation of available potential energy for the Northern Hemisphere circulation. Meridional distributions of heating were also estimated by Newell, Vincent, Dopplick, Ferruzza and Kidson (1970) in their general circulation studies at MIT. These efforts as well as the more recent attempts by Hantel and Peyinghaus (1976), Hantel and Baader (1978), Geller and Avery (1978) and others have used general circulation statistics most notably by Oort and Rasmusson (1971) to infer the climatological heating distribution that must be present to balance the observed distribution of energy transport.

A difference of views over the importance of eddies and mean motion in satisfying balance requirements of the general circulation is summarized by Wallace (1978). No unique answer emerges. To a large degree these

differences emerge from the mathematical-statistical methods used to decompose basic transport processes into mean and eddy components, neither of which by themselves may be uniquely related to boundary processes or internal sources of momentum and energy. For different seasons and different regions the form of circulation realized depends on changing boundary conditions and internal sources of properties, thus complicating the attempts to resolve fundamental questions on the forcing of large scale planetary circulations and the atmosphere's response to differential heating.

The conceptual concepts of exchange processes within an isentropically stratified atmosphere set forth by Sir Napier Shaw (1942) are interesting, particularly in regard to studies of the time-averaged circulation. Regions of heating are energy sources while regions of cooling are energy sinks. Within a time-averaged isentropic structure the mass and energy flux is upward in regions of heating and downward in regions of cooling. For the time-averaged circulation to remain quasi-steady both mass and energy transport must be from the heat source to the heat sink in higher isentropic layers while within lower isentropic layers mass and energy transport must be from the heat sink to the heat source. For steady state conditions the vertically-integrated divergence of the mass transport must vanish while the net transport of energy is from the heat source to the heat sink.

The purpose of this paper is to provide a descriptive analysis of the planetary scale isentropic mass circulation and energy transport forced by the global distribution of differential heating and to establish a link between mass circulation, energy transport and boundary processes in the satisfaction of global energy balance. Some insight into the global distribution of heating will be provided from the patterns of mass and energy transport, although at

the time of preparation of this paper, explicit computations of the diabatic heating have not been completed. In the earlier work of Zillman (1972) and Otto (1974), planetary scale mass circulations associated with the irrotational mode of mass transport were determined from the climatological distribution of diabatic heating. While the fields of the irrotational mode in their work and ours are similar, a detailed comparative discussion of quantitative results has not been included due to the time constraint for completion of this paper for the Bergen Conference.

Quasi-horizontal mass and energy transport

The quasi-horizontal transport of mass and energy embedded within the isentropic structure will be represented by time-averaged mass (ρ) and energy (ν) transport potential ($\overline{\chi}_\rho$ and $\overline{\chi}_\nu$) and stream ($\overline{\psi}_\rho$ and $\overline{\psi}_\nu$) functions through the use of Helmholtz's theorem given by

$$\overline{\rho J \underset{\sim}{U}} = \nabla_\theta \overline{\chi} + \underset{\sim}{k} \times \nabla_\theta \overline{\psi} \qquad (1)$$

where the irrotational and rotational components of the mass transport are defined by

$$(\rho J \underset{\sim}{U})_\chi = \nabla_\theta \chi_\rho \qquad (2)$$

$$(\rho J \underset{\sim}{U})_\psi = \underset{\sim}{k} \times \nabla_\theta \psi_\rho \quad . \qquad (3)$$

Corresponding definitions of irrotational and rotational components of energy transport, $\rho J \underset{\sim}{U}\nu$, are also used in this analysis. The forms of the Poisson equations used to determine $\overline{\chi}$ and $\overline{\psi}$ through vector operations in (1) are

$$\nabla_\theta^2 \overline{\chi}_\rho = \nabla_\theta \cdot (\overline{\rho J \underset{\sim}{U}}) = \delta_\rho$$

$$\nabla_\theta^2 \overline{\chi}_\nu = \nabla_\theta \cdot (\overline{\rho J \underset{\sim}{U} \nu}) = -\delta_\nu \qquad (4)$$

and

$$\nabla_\theta^2 \overline{\psi}_\rho = \underset{\sim}{k} \cdot \nabla_\theta \times (\overline{\rho J \underset{\sim}{U}}) = \zeta_\rho$$

$$\nabla_\theta^2 \overline{\psi}_\nu = \underset{\sim}{k} \cdot \nabla_\theta \times (\overline{\rho J \underset{\sim}{U} \nu}) = \zeta_\nu \quad . \qquad (5)$$

With the divergence and curl of the mass and energy transport specified over the entire sphere from NMC's global Level IIIa FGGE analyses, numerical solutions of the finite difference analogue of the Poisson equations (4) and (5) were performed on a regular five-degree latitude-longitude grid by the method of successive over-relaxation (Young, 1962). From the solutions, $\overline{\chi}$ and $\overline{\psi}$ are uniquely determined with the exception of a constant of integration since no lateral boundary conditions exist for the global domain. For isentropic layers which lie beneath the earth's surface, ρJ is zero from the hydrostatic assumption and from the convention that $p(\theta) = p(\theta_s)$ for $\theta \leq \theta_s$. This convention implies that "underground" isentropic surfaces are contiguous with the earth's surface. For isentropic layers which intersect the earth's surface, the mass ρJ is specified by $p(\theta) - p(\theta_s)$ for all $(\theta_s + \Delta\theta) \geq \theta \geq \theta_s$ where a $\Delta\theta$ of 10 degrees is the vertical extent of the discretized layer used in the analysis. Zillman (1972) presents details on the numerical methods and tests of convergence in using the convention to successfully calculate the mass transport potential from climatological analysis of diabatic heating for

the Southern Hemisphere. Later Otto (1974) successfully completed a similar analysis for the Northern Hemisphere.

Mass balance of the time-averaged state

The time-averaged equation of mass continuity expressed in isentropic coordinates is

$$\frac{\partial}{\partial t_\theta}(\overline{\rho J}) + \nabla_\theta \cdot (\overline{\rho J \underset{\sim}{U}}) + \frac{\partial}{\partial \theta}(\overline{\rho J \dot{\theta}}) = 0 \qquad (6)$$

With the average over a sufficient time interval to invoke the quasi-steady state assumption and use of (4), the balance between the horizontal divergence of the mass transport and the vertical derivative of the diabatic mass flux is given by

$$\nabla_\theta \cdot (\overline{\rho J \underset{\sim}{U}}) = \nabla_\theta^2 \overline{\chi}_\rho = -\frac{\partial}{\partial \theta}(\overline{\rho J \dot{\theta}}) \qquad (7)$$

Horizontal mass convergence (divergence) is balanced by an increase (decrease) of the upward mass flux with elevation in regions of heating or a decrease (increase) of the downward mass flux with elevation in regions of cooling. The mass potential function will tend to be a relative maximum (minimum) in regions of convergence (divergence).

It is important to recognize at this point that the time-averaged quasi-horizontal mass transport (or for that part the transport of any property) defined within different coordinate frameworks may vary. In order to appreciate this point more fully, consider the definition of a time-average

quasi-horizontal mass transport that is applicable to all the meteorological coordinate systems commonly utilized (Johnson and Downey, 1975a; Johnson, 1980).

$$\overline{\rho J_\eta \underset{\sim}{U}} = \overline{\rho \left|\frac{\partial z}{\partial \eta}\right| \underset{\sim}{U}} \tag{8}$$

where (ρJ) is the mass in an incremental volume $\Delta A \Delta \eta$ and $|\partial z/\partial \eta|$ is the Jacobian used to transform height z to a generalized vertical coordinate that may be pressure, potential temperature, sigma, etc.

With the time deviation defined by

$$f' = f - \bar{f} \tag{9}$$

the time-averaged mass transport divides into two components

$$\overline{\rho J_\eta \underset{\sim}{U}} = \overline{(\rho J_\eta)} \, \underset{\sim}{\bar{U}} + \overline{(\rho J_\eta)' \underset{\sim}{U}'} \tag{10}$$

The first component is the product of the time-averages while the second is the product of temporal deviations associated with transient behavior. Both of these components are part of the time-averaged mass transport within a system and both are retained in the definition of mass transport within an isentropic layer. This is an important degree of freedom in capturing the mass and energy transport accomplished by propagating atmospheric phenomena that develop to satisfy balance requirements imposed by differential heating of the atmosphere. On the other hand, the definition of mass transport within a hydrostatic isobaric layer reduces to

$$\overline{\rho \left|\frac{\partial z}{\partial p}\right| \underset{\sim}{U}} = g^{-1} \overline{\underset{\sim}{U}} \qquad (11)$$

since the isobaric mass deviation is identically zero. For all practical purposes, the time-averaged mass transport within Cartesian coordinates also vanishes since the temporal deviations of density are relatively small. In a comparison of transport statistics, it is important to understand that differences in concepts of time-averaged mass and energy transport will emerge that are associated with these degrees of freedom.

Energy balance of the time-averaged state

The time-averaged transport equation for total energy, the sum of the kinetic, gravitational potential and internal (including latent energy of phase changes) energies is (Johnson, 1980)

$$\frac{\partial}{\partial t_\theta}(\overline{\rho Je}) + \nabla_\theta \cdot (\overline{\rho J \underset{\sim}{U} e}) + \frac{\partial}{\partial \theta}(\overline{\rho J \dot{\theta} e}) = \nabla_\theta \cdot [\overline{J(\underset{\approx}{\Pi} \cdot \underset{\sim}{U} + H)}] + \frac{\partial}{\partial \theta}[(\overline{k - \nabla_\theta z) \cdot (\underset{\approx}{\Pi} \cdot \underset{\sim}{U} + H)}] \quad . (12)$$

In this expansion the tendency, quasi-horizontal divergence and vertical derivative of the energy transport balance the sources of energy by boundary pressure and viscous work, and the energy flux associated with radiation and turbulent transfer of sensible and latent energies. This form of the energy equation reveals how changes of total energy within a volume element are determined by boundary energy flux through the surface of the volume element and verifies that the tendency of the time-averaged total energy is determined

by the time-averaged energy flux through the boundary of the isentropic volume element.

A more familiar form of this expression for a hydrostatic atmosphere is given by

$$\frac{\partial}{\partial t_\theta}(\overline{\rho J \nu}) + \nabla_\theta \cdot (\overline{\rho J \underset{\sim}{U} \nu}) + \frac{\partial}{\partial \theta}(\overline{\rho J \dot{\theta} \nu}) = \overline{\rho J (\frac{\partial \psi_M}{\partial t_\theta} + Q_m + \underset{\sim}{U} \cdot \underset{\sim}{F})} \qquad (13)$$

where the sum of the total energy and the "RT" component of work is defined by

$$\nu = e + RT = \psi_M + k \quad . \qquad (14)$$

In this relation the definition of $\psi_M + k$ and $e + RT$ requires that the release of latent energy associated with the phase changes of water vapor be a component of Q_m while the internal energy component of e be defined by $c_v T$ and not include the latent energy of phase changes Lq. In this form of the transport equation, changes of energy are no longer associated with boundary processes. Since boundary pressure work of an ideal gas is directly proportional to internal energy transport, this process is transferred to the left hand side. However, this introduces a term involving the tendency of the Montgomery Stream function on the right hand side that will seldom vanish due to the transient nature of atmospheric phenomena. In addition, the phase change of water vapor represents an internal source of energy to the energy function ν when its component of internal energy is determined by $c_v T$.

Inspection of (12) and (13) suggests that a vertical integration will yield insight into the importance of the horizontal redistribution of energy in association with diabatic and viscous processes at the planetary scale and at

the same time couple these internal processes to the vertically-integrated energy sources and sinks determined by boundary fluxes at the top and bottom of the atmosphere. The result of a vertical integration of (13) and considerable rearrangement in conjunction with assumptions of hydrostatic balance and no transfer of energy by viscous stresses laterally within the atmosphere or across the earth-atmosphere interface (Johnson and Zillman, 1980) yields

$$\int_{\theta_s}^{\theta_T} \frac{\partial}{\partial t_\theta}(\overline{\rho J \nu})d\theta + \int_{\theta_s}^{\theta_T} \nabla_\theta \cdot (\overline{\rho J \underset{\sim}{U} \nu})d\theta = -\int_{\theta_s}^{\theta_T} \overline{\psi_M \frac{\partial}{\partial \theta}(\rho J \dot{\theta})}d\theta + \overline{p_s \frac{\partial z_s}{\partial t}} - \overline{E^z} \quad (15)$$

where $\overline{E^z}$ is the vertically-integrated time-averaged viscous dissipation function. With the additional assumptions of averaging over an appropriate time interval for which the steady state assumption becomes valid and fixing the earth atmosphere interface, (15) reduces to

$$\int_{\theta_s}^{\theta_T} \nabla_\theta \cdot (\overline{\rho J \underset{\sim}{U} \nu})d\theta + \overline{E^z} = -\int_{\theta_s}^{\theta_T} \overline{\psi_M \frac{\partial}{\partial \theta}(\rho J \dot{\theta})}d\theta \quad . \quad (16)$$

This last assumption removes the degree of freedom for energy transfer by boundary pressure work at the earth-atmosphere interface. Over oceans this transfer may not be insignificant in regions of large fetch and systematic wind-driven ocean circulations. In all likelihood, however, the process is a sink of energy from the atmosphere and undoubtedly of lesser magnitude than

the primary terms in (16) that are involved in the quasi-horizontal and vertical redistribution of energy. A vertical integration of the mass continuity equation yields

$$\int_{\theta_s}^{\theta_T} \nabla_\theta \cdot \overline{(\rho J \underset{\sim}{U})} d\theta = -\int_{\theta_s}^{\theta_T} \frac{\partial}{\partial \theta}\overline{(\rho J \frac{d\theta}{dt})} d\theta \quad . \tag{17}$$

A comparison of the forms of (16) and (17) achieved through the analysis within the isentropic framework with a minimum of assumptions reveals the simplicity and similarity of the form of the equations. The dissipation function is always positive and small relative to the divergence of the horizontal transport of energy. Thus, with ψ_M always positive, the sense and scale of the thermally-forced isentropic mass circulation must determine the sense and scale of energy transport. With upper and lower boundary conditions that the energy flux vanishes at θ_T and θ_s($\rho J = 0$ for $\theta < \theta_s$) and an integration by parts, (17) becomes

$$\int_{\theta_s}^{\theta_T} \nabla_\theta \cdot \overline{(\rho J \underset{\sim}{U} \nu)} d\theta + \overline{E^z} = -\int_{\theta_s}^{\theta_T} \overline{\psi_M \frac{\partial}{\partial \theta}(\rho J \dot{\theta})} d\theta = \int_{\theta_s}^{\theta_T} \overline{\rho J \dot{\theta} \frac{\partial \psi_M}{\partial \theta}} \, d\theta \tag{18}$$

This form of the equation states that in regions of heating, energy advection is upward (in a hydrostatic atmosphere $\partial\psi_M/\partial\theta$ is always positive) and the vertically integrated quasi-horizontal energy transport is divergent. In regions of cooling, the energy advection is downward and the vertically integrated energy quasi-horizontal energy transport is convergent. It is important to recognize that vertical integration of (12) yields a result

consistent with (18), the difference being that boundary pressure work in (12) would be on the right hand side of the balance equation while in (18) the boundary pressure work has been transferred to the left hand side. In the case of (12), however, the forcing of the energy transport would have been coupled with the difference between the energy flux at the top and bottom of the atmosphere and no insight would have been revealed into the relation between the structure and modes of quasi-horizontal transport of energy within a stratified atmosphere and the planetary scale distribution of heating.

The mass balance of planetary scale circulation inferred from FGGE level IIIa data

The results for mass and energy transport presented in this study were determined from a FGGE level IIIa data set generated by the National Meteorological Center's (NMC) global data assimilation system. The characteristics of the level IIIa data set and NMC's optimum interpolation data assimilation system are described by NMC's Staff Atmospheric Analysis Branch (1979); Flemming, Kaneskige and McGovern (1979); Fleming, Kaneskige, McGovern and Bryan (1979); Bergman (1979); and McPherson, Bergman, Kistler, Rasck and Gordon (1979).

The isobaric data set consists of twice daily global analysis fields for twelve selected pressure levels from 1000 to 50 mb on a 2.5° latitude-longitude grid. The period of the data set is from December 1978 through November 1979. The meteorological variables of the data set include zonal and meridional wind components, temperature, geopotential height and surface pressure.

Global isentropic analyses were obtained from this data set for the

same grid and observation times by vertical interpolation from isobaric to isentropic coordinates. Gridded fields of the pressure, the zonal and meridional wind components and Montgomery stream function were produced at 16 isentropic levels with 10° vertical resolution. The vertical extent of the isentropic fields varies from Northern to Southern Hemispheres and from month to month since the data is processed by hemispheres and the 16 levels depend explicitly on the minimum surface potential temperature. For any given observation time, the vertical extent always reaches 370 K. This includes nearly all of the planetary tropospheric circulation. In view of the preliminary nature of the level IIIa data set and also of the isentropic diagnostic methods utilized, the mass transport potential and stream functions were generated from a 5° x 5° latitude-longitude grid. Smaller scale details evident in the 2.5° x 2.5° gridded fields are not well resolved; and as a result, the pattern of the large scale transport processes are quite evident. In view of the early nature of the analyses, the discussion of the results in this paper is limited to some degree. Furthermore, only results for January and July will be discussed in detail in order to focus on the winter and summer Asiatic monsoonal circulations. Analyses for April and October are included for comparative purposes.

The mean global transport of mass for January 1979

The isentropic mass and energy transport will be presented for selected levels that capture the nature of the planetary scale monsoonal circulations. The global scale circulations in both summer and winter are described well by the 300-310 K and 340-350 K isentropic levels. At higher latitudes of the Northern Hemisphere, a mass circulation exists within lower levels that

couples the exchange of polar air masses between continental and oceanic regions and is an important feature of its winter monsoon. This exchange primarily occurs within isentropic structure below 300 K; the pattern of which is presented for the 260-270 K, 270-280 K, 280-290 K, and 290-300 K isentropic layers.

The mass transport stream and potential functions for the 300-310 K and 340-350 K isentropic levels for January are displayed on Mercator and polar stereographic projections in Figs. 1, 2, 3 and 4. Negative (dashed lines) and positive (solid lines) values of isopleths of the stream and potential fields are only used to aid in the delineation of maximum and minimum regions of the fields. Since the transport processes are proportional to the gradient of these fields and the constant of integration is arbitrary, the negative and positive values of isopleths are only relative. No physical relevance should be attached a particular value of an isopleth in a comparison of the fields displayed in the different figures.

The mean topography of each isentropic layer of pressure is indicated on the polar stereographic analyses of the mass transport potential for each hemisphere. The sloping nature of isentropic surfaces from the low tropical troposphere to the high polar troposphere is evident in both Figs. 2b and c. In the tropical regions, the 300-310 K layer is located near 800 mb over oceanic regions and near 900 mb over the warmer continental regions of South America and Australia. At polar latitudes, the 300 K surface lies near 500 mb; over the Antarctic continent, the surface is located above 400 mb. The maximum slope of the isentropic surface occurs within the region of intense westerlies circumscribing the polar regions that is evident in Fig. 1b from the gradient of the mass stream function. Within the Northern

Hemisphere circulation, the isentropic layer ascends to 300 mb over polar regions; with the maximum change in elevation from 800 to 400 mb occurring within the region of maximum westerlies (Fig. 1c). From the topography, it is evident that quasi-horizontal transport of mass within this layer couples the low troposphere of the tropical and subtropical regions with the high troposphere of polar latitudes.

The analyses of the topography for the 340-350 K layer in Figs. 4b and c reveal little variation of pressure. For the Southern Hemisphere, the 340-350 K layer lies between the 300 and 200 mb levels while in the Northern Hemisphere the surface lies near 200 mb. Thus, the 340-350 K layer is nearly horizontal and lies within the high tropical-subtropical troposphere and low polar stratosphere. Mass circulations within this layer will link these two regions and provide evidence of stratospheric/tropospheric exchange of mass and other atmospheric properties.

Several interesting features of the westerly circulations in both hemispheres are evident through a contrast of the mass stream functions in the 300-310 K isentropic layer (Fig. 1). The rotational component of the momentum in the Northern and Southern Hemispheres is most intense in middle and higher latitudes. The larger amplitude wave structure of the Northern Hemisphere flow, in contrast with the more zonal flow of the Southern Hemisphere, reflects the influence of continents and oceans in the Northern Hemisphere. The ridging over the Gulf of Alaska, Alaska and western United States and the deep trough over the eastern half of the United States is a feature of the severe winter circulation of 1978-79 over North America. The intense westerlies inferred from the stream function over the eastern portions of the United States is associated with the strong temperature contrast between the

extremely cold polar air during this season in close proximity with the warmer subtropical air. Over the Asiatic mainland and the Western Pacific, the intense stream function gradient is again evidence of the strong westerlies normally occurring during the winter season in this region. In this case, the flow appears to be more zonal during January 1979 and likely reflects lesser meridional exchange than in the North American region. The subtropical anticyclonic circulations in the Southern Hemisphere over the Atlantic, Pacific and Indian Ocean regions are evident in the analyses for the Southern Hemisphere (Fig. 1b). Closed anticyclonic circulations in the Northern Hemisphere (Fig. 1c) are not isolated in the 300 K isentropic layer during the winter season.

The analyses for the mass stream function within the 340-350 K layer (Fig. 3) show strong westerlies in subtropical latitudes of the Northern Hemisphere and a weaker westerly regime extending from tropical latitudes to mid latitudes in the Southern Hemisphere. It is interesting to contrast the poleward displacement of the westerlies within the 300-310 K layer (Fig. 1a) with respect to the westerlies in the 340-350 K layer (Fig. 3a). The results suggest that the westerlies of the subtropical jet stream region occurring at lower latitudes are primarily captured within the 340-350 K layer while the westerlies at the polar jet stream region are displaced towards higher latitudes in the 300-310 K layer. The latitudinal and layered separation of the polar jet stream from its subtropical counterpart within the isentropic structure is enhanced through the definition of the momentum within an isentropic layer. Since the velocity is weighted by the mass within a layer, the sharp cutoff in the gradient of mass stream function at 340-350 K in mid latitudes is a reflection of the small mass in the low polar stratospheric

domain of this layer; thus, the small momentum at these latitudes. The contrast of the meridional extent and relative displacement of the westerlies within each of the two layers is emphasized in the polar stereographic projections in Figs. 1c and 3c.

Differences in the latitudinal domains of the westerlies within each of the two layers are almost certainly due in part to the mass circulations evident in the isentropic zonally-averaged meridional circulations (Townsend and Johnson, 1980). In these meridional circulations, two cells are observed within the large Hadley-type circulation that spans the Northern Hemisphere (shown in total isentropic mass circulation, Fig. 2 of Townsend and Johnson). The westerlies are maintained by poleward transport of angular momentum. The classical ageostrophic Hadley circulation of low latitudes (also shown in Fig. 2 of Townsend and Johnson) is linked with the maintenance of the subtropical jet (Krishnamurti, 1961). The maintenance of the higher latitude intense westerly regime with a polar jet as an entity separate from the subtropical jet is linked with the geostrophic component of the meridional isentropic mass circulation cell in mid-latitudes (Fig. 2 of Townsend and Johnson). Within these latitudes some meridional exchange occurs in conjunction with mid-latitude sources of latent and sensible heat associated with the action of baroclinic waves and extratropical cyclones. As the results for the mid-latitude cell indicate in Figs. 14 and 16 of Townsend and Johnson the mean isentropic meridional transport of angular momentum (as well as the transient transport) is poleward in the region of the polar jet, thereby providing a secondary source of angular momentum for the westerlies within the 300-310 K layers.

The mass transport potential for the 300-310 K and 340-350 K layers

(Figs. 2 and 4) portray coupled mass circulations that link heat sources in regions of convection to other regions of net energy deficit. The strong meridional and zonal variations of the transport potential are evidence of both Hadley-type and Walker-type circulations that span the entire globe. A primary region of energy input indicated in Figs. 2a and 4a occurs in the tropical regions to the northeast of Australia. Within the 300-310 K layer mass convergence occurs while at the 340-350 K layer, the mass transport is divergent. The quasi-circular nature of the 340-350 K potential function that spans radially 6 to 7,000 km indicates that meridional and zonal irrotational components of mass transport in the upper troposphere are approximately equal, thus implying equal importance of the zonal and meridional components of thermodynamically-forced mass and energy transport. The results for the Northern Hemisphere in Fig. 4c illustrate that both the meridional and zonal transport components at these latitudes are linked with convergence over the Sahara and the adjacent eastern Atlantic region. In Fig. 4a the region of mass convergence in the eastern Atlantic links within tropical latitudes another region of mass convergence in the eastern Pacific region just east of Central America and Colombia. The proximity of these two centers of convergence with implied tropospheric subsidence to the center of divergence over Brazil within the 340-350 K layer suggests that the irrotational mode of mass transport links these regions of energy excess and deficit by diabatic processes through thermodynamically-forced mass circulations.

The 340-350 K mass transport potential in Figs. 4a and c shows the link of the mass and energy transport from the tropical regions of the Western Pacific to the Eastern Pacific and Atlantic regions in tropical latitudes of the Southern Hemisphere. From the energy transport inferred from the mass

circulation, the global heat balance of the subtropical anticyclones and desert regions in the tropics are maintained through subsidence in association with the mass convergence in the high troposphere, the primary source of energy being from the regions of convection in the western tropical Pacific. The sense of these global scale isentropic mass circulations agree with Zillman's (1972) and Otto's (1974) results. The sense of the mass circulations and energy transport within tropical latitudes agrees with Flohn's (1971); Krishnamurti's (1971); Krishnamurti, Kanamitsu, Koss and Lee's (1973), and Murakami and Unninayar's (1977) results.

Within the 300-310 K layer, the inverse pattern is evident in Figs. 2b and c. Mass transport is divergent over the Caribbean, Sahara and eastern Atlantic and Pacific regions. Note the smaller scale regions of mass convergence over South merica and over Africa in the vicinity of Madagascar. Both of these are regions of intense convection which also are source regions for the maintenance of the energy balance in addition to the tropical region of the western Pacific.

Another interesting feature in Fig. 2a is the relatively strong equatorward meridional mass transport from the Southern Hemisphere circumpolar vortex and Eastern Asia into the source region of convection in the western Pacific. Note that the divergent component of the mass transport suggests a strong tropical-extratropical coupling in both the Southern and Northern Hemispheres. Mass and energy are transported to lower latitudes in these sectors. In the Northern Hemisphere, the divergent mode of mass transport just east of the Phillipines is a part of the Asiatic winter monsoonal flow within the low troposphere through which the atmosphere acquires sensible and latent energies in its equatorward motion (A link of this feature with

transport within lower isentropic layers is established in the next paragraph). This mass and energy transport from the higher latitudes is in effect a source of heat through convergence of energy transport to the low tropical troposphere that helps to maintain a vertical structure favorable for the deep convection in those regions. Concepts of atmospheric circulation based on ideas that the maintenance of convection within the tropics occurs through "in situ" sources of latent and sensible energies are oversimplified.

The irrotational components of the isentropic mass circulations presented for the Northern Hemisphere in Fig. 5 for the four lower isentropic layers ranging from 260-270 K to 290-300 K provide evidence of exchange of polar air between continental and oceanic regions through monsoonal circulations in the winter season. Within the lower layers, 260 K and 270 K (Figs. 5a and b), the mass transport is divergent over Arctic regions and convergent over the oceanic regions just east of the Asian and North American continents. The strong gradient of the mass transport potential over Japan, the Northern Pacific, as well as Nova Scotia and the Northern Atlantic is evidence of winter monsoonal flow with polar air moving equatorward and zonally from continental regions to the oceanic areas of mass convergence over the Gulf Stream and Japanese current. Within these areas, strong sensible and latent heat release create upward vertical mass flux while the downward mass flux over the Artic regions occurs in association with the net energy loss due to the excess of the sink of energy by infrared emission over other energy sources. Within the 280 K and 290 K layers (Figs. 5c and d), strong mass divergence exists above the oceanic regions of convergence beneath 280 K while convergence exists over Arctic regions. Thus, energy is exported from the heat sources in the oceanic regions to the Arctic regions where air

radiatively cools within the Arctic air masses. In an analysis of the time-averaged circulation and energetics of the Northern Hemisphere winter Blackmon, Wallace, Lau and Mullen (1977), and Lau (1978, 1979) emphasize the importance of planetary scale heat sources and sinks in the forcing of time-mean jet streams off the east coasts of Asia and North America. They suggest that thermally direct and indirect (time) mean meridional circulations are important with respect to the forcing and maintenance of these time-mean jet streams. In their analysis, direct meridional circulations over eastern Asia and North America are linked with heat sinks over the respective continents in winter while indirect meridional circulations over the western regions of the Pacific and Atlantic Oceans are linked with the heat sources associated with the Aleutian and Icelandic lows and the large scale subsidence in subtropical oceanic anticyclones. However, the model of the time-mean jet stream does not establish a direct link between the energy transport from the heat source region over oceans to the heat sink region over polar regions by this scale of circulation to maintain energy balance.

Through the isentropic analysis some additional facts emerge. The three-dimensional structure of the mass circulations beneath 300 K within the polar and mid-latitudes is in part responsible for the maintenance of the polar westerlies on the 300 K surface. Note from the zonally-averaged mass circulation and the meridional heating distribution presented by Townsend and Johnson (1980) in their Figs. 2, 9 and 10, the heating maximum near 40-50°N is linked with mid-latitude oceanic sources of energy to polar air masses and an embedded secondary Hadley-type cell poleward of 40°N. As discussed by Townsend and Johnson, the resulting mass circulation is linked to the poleward transport of angular momentum within the baroclinic structures of the mid

latitudes. Within Eliassen's (1951) perspective of the forcing of a vortex, westerlies associated with the polar jet stream stem, in part, from these mass circulations being forced by a combination of differential heating and torques (Gallimore and Johnson, 1977). The poleward geostrophic mode of mass transport that exists within the 290-300 K layer is linked with negative pressure torques that force poleward motion while below 280 K positive pressure torques force mass transport equatorward. As a consequence, absolute angular momentum is transported poleward within this thermodynamically-forced mass circulation, and at the same time also transferred from the upper to the lower branch of the mass circulation through the action of pressure torques and pressure stresses (Johnson and Downey, 1975a and b). This circulation is basic to the maintenance of the westerlies of the polar jet stream. If the heat source of latent and sensible energies were absent in these regions, the polar jet stream with its transient nature of angular momentum transport would be absent or of a different character.

The mean global transport of mass for July 1979

The mass transport potential and stream functions for the 300-310 K and 340-350 K isentropic surfaces, July 1979, are presented in Figs. 6, 7, 8 and 9. At the 300-310 K layer, the intense gradient of the mass stream function in Fig. 6a is evidence of the strong westerlies of the Southern Hemisphere circumpolar vortex. The pressure analyses shown in Fig. 7b again indicate the slope of this isentropic layer from below 800 mb in tropical latitudes to 300 mb over the Antarctic continent. The maximum slope in mid-latitudes of the Southern Hemisphere is evidence of the baroclinic support to the westerlies of the circumpolar vortex. Distinct anticyclonic circulations are

indicated in the subtropics reaching from New Zealand across South America to the eastern Atlantic (Figs. 6a and b). The Pacific and Atlantic subtropical anticyclones are well developed in the Northern Hemisphere (Figs. 6a and c). The anticyclonic circulation in the low-equatorial troposphere of the Indian Ocean region (Fig. 6a), is part of the rotational component of the low-level mass circulation. Note the easterly current at 15°S reaching from the eastern Indian Ocean to near Madagascar, its anticyclonic curvature to the north and its further turning to the northeast after crossing the equator. Embedded within this low tropospheric circulation within the 300-310 K layer is the Somali jet that transports heat and moisture for the maintenance of the convection in the Indian monsoon.

The westerlies in the high latitudes of the Northern Hemisphere, while weak, are most pronounced from the Pacific Ocean across Northern Canada and the Northern Atlantic (Figs. 6a and c). Over the Siberian portion of the Asiatic continent the gradient is extremely weak, thus indicating minimal average circulation at these levels. The stream function in Fig. 6c indicates the location of a weak cyclonic circulation over the high polar regions that is displaced towards the North American continent.

The mass stream function for the 340-350 K isentropic level in July (Fig. 8) shows a distinct anticyclonic circulation over the region from Southeastern Asia to Northern Africa that captures the mean position of the Tropical Easterly Jet. Another anticyclonic circulation is located over the Southern United States-Mexican region. The primary circulation feature of the circumpolar vortex at this level is the belt of the westerlies over Southern Africa and Australia and the Chile-Argentina portions of South America. This belt of westerlies within the 340K-350 K layer is displaced equatorward to

some extent to the westerlies within the 300-310 K layer and lies above the anticyclonic circulations of the lower troposphere. Just like the analysis for the Northern Hemisphere, this latitudinal displacement of the westerlies and the mid-latitude Hadley-type cell within the isentropic mass circulation (Townsend and Johnson, 1980) suggests a distinction between westerlies at higher latitudes and the subtropical westerlies at lower latitudes. However, in this case the secondary Hadley-type cell indicated in the results of Townsend and Johnson (1980, Fig. 4) is much weaker in comparison with its Northern Hemisphere counterpart and the distinction is less pronounced. This result suggests that diabatic heat sources in mid-latitudes of the Southern Hemisphere are relatively less important than their Northern Hemisphere counterpart; although it is possible that this mass transport within the lower isentropic layers of the Southern Hemisphere was not resolved well in this data set.

The mass transport potential at the 300-310 K level (Fig. 7a) shows the dominance of the Asiatic monsoon. The center of convergence appears to be displaced further east than anticipated and may well be associated with the lateness and erratic monsoon in India during July 1979. The region of strongest irrotational mode of mass transport towards the maximum of the potential function over the South China Sea occurs from the southwest over the Indian Ocean and Arabian Sea. Intense irrotational mass transport towards the same center also occurs throughout Malaysia and the equatorial regions of the Western Pacific. A secondary region of mass convergence is located over the Caribbean and Central America. Within the subtropical latitudes of the Southern Hemisphere, the centers of divergence of the mass transport are located over the eastern portion of the Pacific high and over the Southern

Atlantic-African region. From the relative intensity and scale of the regions of the irrotational mass transport the results (Fig. 6a) show that isentropic mass circulations link these centers of divergence with the center of convergence over the South China Sea and illustrate the global nature of the mass circulation that is dominated by the Asiatic monsoon.

At the 340-350 K isentropic level (Fig. 9), the primary center of mass divergence over southeastern Asia is located over the lower level of convergence within the 300-310 K layer. A secondary region of divergence occurs over the Southwestern United States and Mexico. The regions of convergence in the Southern Atlantic and Eastern Pacific of the Southern Hemisphere lie over the regions of divergence with the 300-310 K layer.

It should be emphasized that these mass circulations primarily determine the sense of energy transport. The results of (16) through (18) dictate that energy from convection in the region of the Asiatic monsoon is advected vertically to be exported to higher latitudes of both hemispheres and also longitudinally to the Eastern Pacific and Atlantic sectors of the Southern Hemisphere. At the same time, the convergence of mass with the 300-310 K layer in the lower tropical troposphere over Southeastern Asia provides a source of energy that helps to maintain the convection in these areas. Since this air, in part, lies within the planetary boundary layer in the tropical regions, the mass convergence is also linked with convergence of water vapor transport that supplies the latent energy during the excitation of convection. There is little doubt that the structure of the thermodynamically-forced mass circulation in the Southern Asiatic Indian Ocean region plays a primary role in the nature and structure of the entire planetary circulation through quasi-horizontal mass and energy transport.

The mean global transport of energy for July 1979

The results for the energy balance of the time-averaged state within isentropic coordinates summarized earlier indicate that the irrotational component of the mass circulation determines the sense and scale of the energy transport. From a physical viewpoint, the time-averaged isentropic structure is relatively steady. Thus within this structure diabatic heating is offset by pseudo-adiabatic cooling in energy source regions and diabatic cooling is offset by adiabatic heating primarily through vertical motions. At the same time, mass and energy are transported quasi-horizontally in higher-valued isentropic layers from energy source regions to energy sink regions while in lower-valued isentropic layers both mass and energy are transported quasi-horizontally from energy sink regions to energy source regions. Within the time-averaged structure, the branch of the mass circulation in the higher-valued isentropic layer transports more energy from the heat source region to the heat sink region than the branch in the lower-valued isentropic layer returns. Thus, a net energy transport from the heat source and heat sink regions results even though the net mass transport vanishes. Furthermore, since the divergence of the rotational component of energy transport vanishes and does not produce any net energy transport between heat source and sink, the solutions for the energy transport potential from the observed data determine the pattern and intensity of the global redistribution of energy. This result established by (16) through (18) is independent of whether or not the mode of quasi-horizontal energy transport is by time-averaged or transient components of atmospheric motion. The divergence of the energy transport vector may be partitioned into time-mean and transient components given by

$$\nabla_\theta^2 \overline{\chi} = \nabla_\theta \cdot (\overline{\rho J \underset{\sim}{U} v}) = \nabla_\theta \cdot [\overline{\rho J}(\hat{\underset{\sim}{U}}\hat{v} + \widehat{\underset{\sim}{U}^* v^*})] \tag{19}$$

where the time mass weighted average and its deviation are defined by

$$\hat{f} = \overline{\rho J f}/\overline{\rho J}$$

$$f^* = f - \hat{f} \quad . \tag{20}$$

If patterns of energy transport are like the patterns of mass transport, one can tentatively conclude that the transient component of isentropic energy transport is of lesser importance. If the patterns differ, then the transient component of energy transport increases in relative importance.

The energy stream and potential functions from the 300-310 K and 340-350 K isentropic layers are presented for July 1979 in Figs. 10 through 13. A comparison of the patterns of the modes of energy transport in each of the figures for energy transport with corresponding figures of mass transport reveals that, except for scaling, the time-averaged mass circulation determines the time-averaged energy transport. In a few figures, minor variations exist in the local patterns that may be in part or entirely associated with differences in isopleth values and intervals that result from specifying mass transport in one case and energy transport in the other. Because of the remarkable similarity of the rotational and irrotational modes of mass and energy transport, the energy transport corresponding with mass transport for the other months described earlier will not be presented nor will an extensive discussion of results for energy transport be given in this paper.

The patterns of the energy potential functions in Figs. 11 and 13 again emphasize the dominance of the summer Asiatic monsoon in the planetary scale transport of energy. The low tropospheric convergence of energy transport over India and Southeast Asia within the 300-310 K layer is capped by upper tropospheric divergence of energy transport within the 340-350 K layer. In this region energy is advected vertically and exported quasi-horizontally by the isentropic mass circulation. The other source region of energy is over the Caribbean and Central America. Both of these source regions of energy are linked by zonal and meridional components of net energy transport in association with Walker and Hadley-type mass circulations to heat sink regions in higher latitudes and in subtropical anticyclonic circulations. The energy transport results establish that within the isentropic structure the irrotational modes of mass and energy transport are not confined to lower latitudes but that planetary scales of atmospheric circulation develop in direct response to the differential heating at the global scale to satisfy energy balance. Preliminary analysis indicates that the transient component of isentropic energy transport is minimal if not negligible, a result consistent with Zillman's (1972) earlier analysis.

As emphasized by Johnson and Downey (1975a), the rotational and irrotational modes of mass and energy transport in conjunction with mean and eddy components will vary when analyzed within different coordinate frameworks. However, the net vertically integrated horizontal transport of any property from one region to another must be independent of the coordinate system used in the analysis. Thus in this case, the results for the vertical integrated isentropic mass and energy transport must be identical with like analysis in other coordinate systems even though statistical and mathematical

decomposition of transport processes will at times be different. It should also be emphasized that systematic isentropic mass circulations embedded in the atmosphere exist which are thermodynamically forced and serve to satisfy global energy balance requirements. This fact becomes independent of the coordinate system used in the analysis since it is a mean physical circulation; however, the only way that such circulations may be isolated within latitudinal regions when geostrophy prevails is through the use of the isentropic framework.

The mean global transport for April and October 1979

The irrotational and rotational modes of mass transport for April and October 1979 are presented in Figs. 14 through 21. The primary purpose for the inclusion of these results is to illustrate the seasonal shift of the region of primary heat source region in Indonesia-Southeast Asia across the equator in the annual course of events. Note in April (Figs. 15a and 17a) that the center of mass convergence within the 300-310 K layer and divergence within the 340-350 K layer lies over the equator north of New Guinea. A great deal of symmetry about the equator and the center meridian occurs in this feature. The symmetry about the two lines suggests again as a first approximation that the Walker-type and Hadley-type circulations within the isentropic structure are of relatively equal importance in transport of energy from source to sink regions. Less symmetry occurs in October when the center of mass convergence within the 300-310 K layer lies north of the equator and east of the Phillipines.

In the rotational mode of mass transport (portrayed in Figs. 14, 16, 18 and 20), the circumpolar westerlies are approximately equal in intensity

except for the 300-310 K level where the Southern Hemisphere westerly circulation is somewhat more intense. Well-developed anticyclonic circulations are found within the 300-310 K layer. The only anticyclonic circulation at the 340 K layer is located over the Phillipines in April and to a large degree must be associated with the low tropospheric heat source associated with convection.

Summary and conclusions

The results presented herein are from a preliminary analysis of the planetary scale mass and energy transport determined from a FGGE Level IIIa data set generated by the National Meteorological Center (NMC). The transport was partitioned into rotational and irrotational modes in order to isolate the thermodynamically-forced planetary scale circulations that link regions of heat sources and heat sinks. The results are presented in descriptive form in order to focus on an overview of global scale mass and energy transport that were observed during FGGE and to illustrate the consistency of the NMC information generated by optimum interpolation. The descriptive discussion is also useful to gain familiarity with the nature of planetary scale mass and energy exchange within the isentropic framework.

The results verify the global nature of monsoonal circulations that are linked to the planetary scale of differential heating. The primary planetary source region of energy in the region of Indonesia-Phillipines-Southeast Asia is linked through quasi-horizontal mass transport with primary sink regions of energy in the two circumpolar vortices, the Sahara and subtropical anticyclonic circulations. During the summer seasons other secondary source regions of energy occur over Brazil, the Carribean and Africa. This primary

center of the source of energy in the Indonesia-Southeast Asia area moves seasonally from one hemisphere to the other. In January it is located southeast of New Guinea and northeast of Australia over the Pacific Islands, by April it shifts due north to a position over the Equator, by July it moves northeastward to the South China Sea and by October it moves eastward to a position east of the Phillipines and north of New Guinea. Regions of energy loss and corresponding centers of circulation also seasonally shift position and vary in intensity. A more extensive analysis will serve to establish the structure of isentropic transport processes and corresponding circulation within these centers of action throughout the course of the year.

Analysis also revealed a polar mid-latitude mass circulation within the 260-300 K isentropic layers. The energy source regions associated with sensible and latent heating over mid-latitude oceanic regions east of the Asian and North American continents were linked by an irrotational mode of mass and energy transport with the heat sink region over polar latitudes. The differential heating within these latitudes is responsible for the mid-high latitude Hadley-type cell embedded in the isentropic zonally-averaged mass circulation (Townsend and Johnson, 1980) and in part forces mean and transient modes of poleward angular momentum transport. This angular momentum transport helps to intensify and maintain the relative high easterly momentum in the mid and lower troposphere of these regions. The counterpart in the winter Southern Hemisphere, which was much weaker, does not appear to develop to the same level of intensity as observed in the Northern Hemisphere; this is most likely due to the lack of a mid-latitude heat source associated with the land-ocean contrast in the westerlies and the eastward movement of extremely cold polar air masses over relatively warm oceans. It could also be due to an

inability to resolve the baroclinic structure of middle latitude transport processes in the Southern Hemisphere due to sparsity of information.

The relations between 1) the global distribution of boundary energy flux through the earth's surface and the top of the atmosphere, 2) heat sources and sinks internal to the atmosphere and 3) planetary scale mass and energy transport processes within the isentropic stratification of the atmosphere has been broadly established from transport theory and results. Net heating within a given region and net cooling in another region in association with differences in boundary flux through the earth's surface and the top of the atmosphere result in net energy transport from the source to the sink region, a result basic to thermally-forced circulations. The net energy transport is realized from the condition that more energy is transported by a branch of a circulation in higher-valued isentropic layers from the heat source to the heat sink than is returned by a branch of circulation within lower-valued isentropic layers. At the same time no net mass change occurs. Thus a steady time-averaged circulation that is embedded in the isentropic structure may be realized.

To a high degree of approximation this global exchange characterizes the mass and energy transport of the planetary scale circulation within climatic or multi-annual time scales. Within monthly and seasonally-averaged time scales such exchange is undoubtedly valid to a first degree of approximation in conjunction with seasonal variations of differential heating and corresponding changes in the intensity and position of the centers of action. The variations in intensity and/or position of circumpolar vortices and subtropical anticyclones appear to be consistent with the planetary scale monsoonal circulations that develop in direct response to the differential

heating. The mass and energy transport by global monsoonal circulations would appear to be a basic component of the transport processes linked with observed teleconnections. It must be recognized that differential heating is determined by the external process of boundary energy flux and by the internal process of latent energy release within the resulting circulation. Since latent energy release occurs through mass circulations that are forced internally within the atmosphere through momentum exchange, the atmosphere's response to differential heating is neither separately determined by external forcing or by internal dynamical mechanisms within which the momentum balance is fundamental. Future work will be addressed to the problem of how momentum balance is achieved and maintained in the realization of thermally forced mass circulations.

It is important to realize that within the isentropic structure, the scale and intensity of mass and energy transport can be related directly to the scale and intensity of differential heating and that the transient component of energy transport within isentropic layers is minimal while its counterpart in momentum is not. This result is linked with 1) the classical condition that steady adiabatic inviscid motion must be tangent to both the entropy and energy surfaces and 2) the condition emphasized earlier in the discussion that, in the time-averaged isentropic balance of energy, quasi-horizontal transport is related to the distribution of the time-averaged vertical energy flux. No similar constraint exists for the momentum balance. In the atmosphere large scale quasi-horizontal mass and energy transport between regions of heat sources and sinks tends to be adiabatic and inviscid. Since the statistical partition of transport processes within the isentropic structure provides for a mean mode of transport by both geostrophic and

ageostrophic components of motion, the mode of mean transport of energy which is associated with the thermally-forced mean mass circulation can directly respond to satisfy energy balance requirements everywhere. The irrotational mode of mass and energy transport that links energy sources and sinks may be by ageostrophic motion within circulations at low latitudes and geostrophic motion at higher latitudes. Where the flow transitions, a handover in the component of transport from ageostrophic to geostrophic motion will occur that does not entail a change in the scale of quasi-horizontal transport within an isentropic layer, thus allowing the establishment of a direct link between the global scale of differential heating and the scale of response within the context of a temporally or zonally-averaged mean mass circulation. This feature of isentropic analysis of planetary scale transport processes is important in establishing the relation between changes in thermodynamic forcing and in the response of planetary scale circulations, particularly for longer time scales associated with seasonal and climatic variations.

Acknowledgments

We express our appreciation to Thomas Whittaker and Richard Selin for their computer programming and data processing assistance, to John Stremikis for his guidance in preparing the figures, and to Nancy Malz and Jean Johnson for typing the manuscript. This research was supported by The National Science Foundation, Atmospheric Research Section Grant #ATM77-22976, and Climate Dynamics Research Section Grant #ATM78-22384. The second author (Capt Ronald D. Townsend) is pleased to acknowledge the research opportunity provided by the U. S. Air Force Institute of Technology.

List of Symbols

J	Jacobian for transformation of vertical coordinate to potential temperature $\lvert\frac{\partial z}{\partial \theta}\rvert$
J_η	Jacobian for transformation of vertical coordinate to generalized coordinate $\lvert\frac{\partial z}{\partial \eta}\rvert$
Q_m	Heat addition per unit mass
E^2	Vertically integrated viscous generation of internal energy
e	Total energy, the sum of kinetic, internal and gravitational energies
ν	Total energy plus RT component of work
f	Arbitrary function
g	Acceleration due to gravity
z	Height
k	Kinetic energy
p	Pressure, quasi-horizontal surface
t	Time
η	Generalized vertical coordinate; quasi-horizontal surface
θ	Potential temperature, quasi-horizontal surface
δ	Divergence of vector transport defined by (4)
ζ	Vertical component of curl of vector transport defined by (5)
ψ_M	Montgomery stream function
ρ	Density
χ	Transport potential function
ψ	Transport stream function

Subscripts

ρ	Designates mass transport
ν	Designates energy transport
χ	Designates irrotational component
ψ	Designates rotational component
s	Surface of the earth
η	Denotes generalized coordinate system
θ	Denotes isentropic coordinate system

Vectors

$\underset{\sim}{F}$	Frictional force
$\underset{\sim}{H}$	Energy flux vector
$\underset{\sim}{U}$	Wind velocity
$\underset{\sim}{k}$	Unit vector of local vertical coordinate

Tensors

$\underline{\underline{\Pi}}$	Stress tensor

Operators

$\overline{f}$ **Time average defined by** $\frac{1}{T}\int_0^T f\,dt$

f' **Time deviation defined by** $f - \overline{f}$

$\hat{f}$ **Mass-weighted time average defined by** $\overline{\rho J f}/\overline{\rho J}$

f^* **Mass-weighted time deviation defined by** $f - \hat{f}$

$\cdot$ **Substantial derivative with respect to time**

$\frac{\partial}{\partial t_\theta}$ **Local time derivative in isentropic coordinates**

∇_θ **Quasi-horizontal del operator for isentropic coordinate system defined by** $\nabla_\theta = \underset{\sim}{i}\frac{\partial}{\partial x_\theta} + \underset{\sim}{j}\frac{\partial}{\partial y_\theta}$

∇_θ^2 **Quasi-horizontal Laplacian operator in isentropic coordinate system**

References

Bergman, K. H., 1979: A multivariate optimum interpolation analysis system of temperature and wind fields. Mon. Wea. Rev., Vol. 107, 1423-1444.

Blackmon, M. L., J. M. Wallace, N.-C. Lau, and S. L. Mullen, 1977: An observational study of the Northern Hemisphere wintertime circulation. J. Atmos. Sci., Vol. 34, 1040-1053.

Clapp, P. F., 1961: Normal heat sources and sinks in the lower troposphere in winter. Mon. Wea. Rev., Vol. 89, No. 5, 147-162.

Eliassen, A., 1951: Slow thermally or frictionally controlled meridional circulation in a circular vortex. Astrophys. Norv., Vol. 5, 19-60.

Fleming. R. J., T. M. Kaneskige, and W. E. McGovern, 1979a: The Global Weather Experiment I. The observational phase through the first special observing period. Bull. Am. Meteorol. Soc., Vol. 60, 649-659.

Fleming, R. J., T. M. Kaneskige, W. E. McGovern, and T. E. Bryan, 1979b: The Global Weather Experiment II. The second special observing period. Bull. Am. Meteorol. Soc., Vol. 60, 1316-1322.

Flohn, H., 1971: Tropical circulation pattern. Bonner Meteorolgische Abhandlungen, 15, 55 pp.

Gallimore, R. G., 1973: A diagnostic model of the zonally averaged circulation in isentropic coordinates. Ph.D. Thesis, Univ. of Wisconsin, Madison, WI, 294 pp.

Gallimore, R. G., and D. R. Johnson, 1977: The forcing of the meridional circulation of the isentropic zonally averaged circumpolar vortex. Scientific Report to NSF. Isentropic numerical models: Results on model development for zonally averaged and secondary circulations. Dept. of Meteor. and SSEC, Univ. of Wisconsin, Madison, WI, 89-126.

Geller, M. A., and S. K. Avery, 1978: Northern Hemisphere distributions of diabatic heating in the troposphere derived from general circulation data. Mon. Wea. Rev., Vol. 106, 629-636.

Hantel, H., and W. Peyinghaus, 1976: Vertical heat flux components in the northern atmosphere. Mon. Wea. Rev., Vol. 104, 168-179.

Hantel, M., and H.-R. Baader, 1978: Diabatic heating climatology of the zonal atmosphere. J. Atmos. Sci., Vol, 35, 1180-1189.

Johnson, D. R., and W. K. Downey, 1975a: Azimuthally averaged transport equations for storms: Quasi-Lagrangian diagnostics 1. Mon. Wea. Rev., Vol. 103, 967-979.

Johnson, D. R., and W. K. Downey, 1975b: The absolute angular momentum of storms: Quasi-Lagrangian diagnostics 2. Mon. Wea. Rev., Vol. 103, 1063-1076.

Johnson, D. R., 1980: A generalized transport equation for use with meteorological coordinate systems. Mon. Wea. Rev., Vol. 108, No. 6. In press.

Johnson, D. R., and J. W. Zillman, 1980: Thermally-forced planetary scale circulations and atmospheric transport processes. Manuscript in preparation.

Krishnamurti, T. N., 1961: The subtropical jet stream of winter. Journal of Meteorology, Vol. 18, 172-191.

Krishnamurti, T. N., 1971: Tropical east-west circulation during the northern summer. J. Atmos. Sci., Vol. 28, 1342-1347.

Krishnamurti, T. N., M. Kanamitsu, W. J. Koss, and J. D. Lee, 1973: Tropical east-west circulation during the northern winter. J. Atmos. Sci., Vol. 30, 780-787.

Lau, N.-C., 1978: On the three-dimensional structure of the observed transient eddy statistics of the Northern Hemisphere winter-time circulation. J. Atmos. Sci., 35, 1900-1923.

Lau, N.-C., 1979: The observed structure of tropospheric stationary waves and the local balances of vorticity and heat. J. Atmos. Sci., Vol. 36, 996-1016.

McPherson, R. D., K. H. Bergman, R. E. Kistler, G. E. Rasck, and D. S. Gordon, 1979: The NMC operational global data assimilation system. Mon. Wea. Rev., Vol. 107, 1445-1461.

Murakami, T., and M. S. Unninayar, 1977: Atmospheric circulation during December 1970 through February 1971. Mon. Wea. Rev., Vol. 106, 1024-1038.

NMC Staff Atmospheric Analysis Branch, 1979: Characteristics of FGGE Level IIIa data sets from the NMC global data assimilation system. AMS Preprint Volume, Fourth Conference on Numerical Weather Prediction, October 29-November 1, 1979, Silver Spring, Maryland, 331-334.

Newell, R. E., D. G. Vincent, T. D. Dopplick, D. Farruza, and J. W. Kidson, 1970: The energy balance of the global atmosphere. The Global Circulation of the Atmosphere, Royal Meteorological Society, London, 255 pp.

Oort, A. H., and E. M. Rasmusson, 1971: Atmospheric circulation statistics. NOAA Professional Paper, 5, U. S. Dept. of Commerce, 323 pp.

Otto, B. L., 1974: Isentropically time-averaged mass circulations in the Northern Hemisphere. M.S. Thesis, Univ. of Wisconsin, Madison, WI, 95 pp.

Shaw, Sir Napier, 1942: Manual of Meteorology, The Physical Processes of Weather, Vol. III, Cambridge University Press, 445 pp.

Townsend, R. D., and D. R. Johnson, 1980: The mass and angular momentum balance of the zonally-averaged global circulation. Paper to be presented at the International Conference on Preliminary FGGE Data Analysis and Results, June 23-27, 1980, Bergen, Norway.

Wallace, J. M., 1978: The general circulation: Theory, modeling, and observations. Published notes from a National Center for Atmospheric Research/Advanced Study Program Colloquium, Summer 1978, Boulder, Colorado, 1-24.

Wiin-Nielsen, A., and J. A. Brown, Jr., 1962: On diagnostic computations of atmospheric heat sources and sinks and the generation of available potential energy. Proceedings of the International Symposium on Numerical Weather Prediction, Meteorological Society of Japan, Tokyo, 519-613.

Young, D., 1962: The numerical solution of elliptic and parabolic differential equations. In J. Todd (ed.), Survey of Numerical Analysis, McGraw-Hill, New York, 380-438.

Zillman, J. W., 1972: Isentropically time-averaged mass circulations in the Southern Hemisphere. Ph.D. Thesis, Univ. of Wisconsin, Madison, WI, 205 pp.

Figure Legends

Figure 1. Mass stream function for the 300-310 K isentropic layer of January 1979 on global Mercator (A) and Southern (B) and Northern (C) Hemisphere polar stereographic projections (units, 10^9 kg K^{-1} s^{-1}). Rotational component of isentropic mass transport, $\rho J \underset{\sim}{U}_\psi$, is parallel to the contours with lower values to the left.

Figure 2. Mass transport potential (solid and dashed lines in (A), solid lines only in (B) and (C)) for the 300-310 K isentropic layer of January 1979 on global Mercator (A) and Southern (B) and Northern (C) Hemisphere polar stereographic projections (units, 10^8 kg K^{-1} s^{-1}). Plus and minus signs indicate relative maxima and minima, respectively, in the potential field. Irrotational component of isentropic mass transport, $\rho J \underset{\sim}{U}_\chi$, is perpendicular to the contours from lower to higher values. Dashed contours in (B) and (C) represent the mean pressure of the isentropic layer (units, 10^2 mb).

Figure 3. Mass stream function for the 340-350 K isentropic layer of January 1979. Format and legend same as Fig. 1.

Figure 4. Mass transport potential for the 340-350 K isentropic layer of January 1979. Format and legend same as Fig. 2. The mean pressure of the layer is between 300 and 200 mb in B.

Figure 5. Mass transport potential (solid contours) for 260-270 K (A), 270-280 K (B), 280-290 K (C), and 290-300 K (D) isentropic layers for the Northern Hemisphere of January 1979 (units, 10^8 kg K^{-1} s^{-1}). The potential field is contoured only where the isentropic layer is above the earth's surface. Plus and minus signs indicate relative maxima and minima, respectively, in the potential field. Irrotational component of isentropic mass transport, $\rho J \underset{\sim}{U}_\chi$, is perpendicular to the contours from lower to higher values. Dashed contours represent the mean pressure of the isentropic layer (units, 10^2 mb).

Figure 6. Mass stream function for the 300-310 K isentropic layer of July 1979. Format and legend same as Fig. 1.

Figure 7. Mass transport potential for the 300-310 K isentropic layer of July 1979. Format and legend same as Fig. 2.

Figure 8. Mass stream function for the 340-350 K isentropic layer of July 1979. Format and legend same as Fig. 1.

Figure 9. Mass transport potential for the 340-350 K isentropic layer of July 1979. Format and legend same as Fig. 2.

Figure 10. Energy stream function for the 300-310 K isentropic layer of July 1979 on global Mercator (A) and Southern (B) and Northern (C) Hemisphere polar stereographic projections (units, 10^{14} J K^{-1} s^{-1}). Rotational component of isentropic energy transport, $\rho J \underset{\sim}{U}_\psi$, is parallel to the contours with lower values to the left.

Figure 11. Energy transport potential (solid and dashed lines in (A), solid lines only in (B) and (C)) for the 300-310 K isentropic layer of July 1979 on global Mercator (A) and Southern (B) and Northern (C) Hemisphere polar stereographic projections (units, 10^{14} J K^{-1} s^{-1}). Plus and minus signs indicate relative maxima and minima, respectively, in the potential field. Irrotational component of isentropic energy transport, $\rho J \underset{\sim}{U} \chi$, is perpendicular to the contours from lower to higher values. Dashed contours in (B) and (C) represent the mean pressure of the isentropic layer (units, 10^2 mb).

Figure 12. Energy stream function for the 340-350 K isentropic layer of July 1979. Format and legend same as Fig. 10.

Figure 13. Energy transport potential for the 340-350 K isentropic layer of July 1979. Format and legend same as Fig. 11 except potential units are 10^{13} J K^{-1} s^{-1}.

Figure 14. Mass stream function for the 300-310 K isentropic layer of April 1979. Format and legend same as Fig. 1.

Figure 15. Mass transport potential for the 300-310 K isentropic layer of April 1979. Format and legend same as Fig. 2.

Figure 16. Mass stream function for the 340-350 K isentropic layer of April 1979. Format and legend same as Fig. 1.

Figure 17. Mass transport potential for the 340-350 K isentropic layer of April 1979. Format and legend same as Fig. 2.

Figure 18. Mass stream function for the 300-310 K isentropic layer of October 1979. Format and legend same as Fig. 1.

Figure 19. Mass transport potential for the 300-310 K isentropic layer of October 1979. Format and legend same as Fig. 2.

Figure 20. Mass stream function for the 340-350 K isentropic layer of October 1979. Format and legend same as Fig. 1.

Figure 21. Mass transport potential for the 340-350 K isentropic layer of October 1979. Format and legend same as Fig. 2.

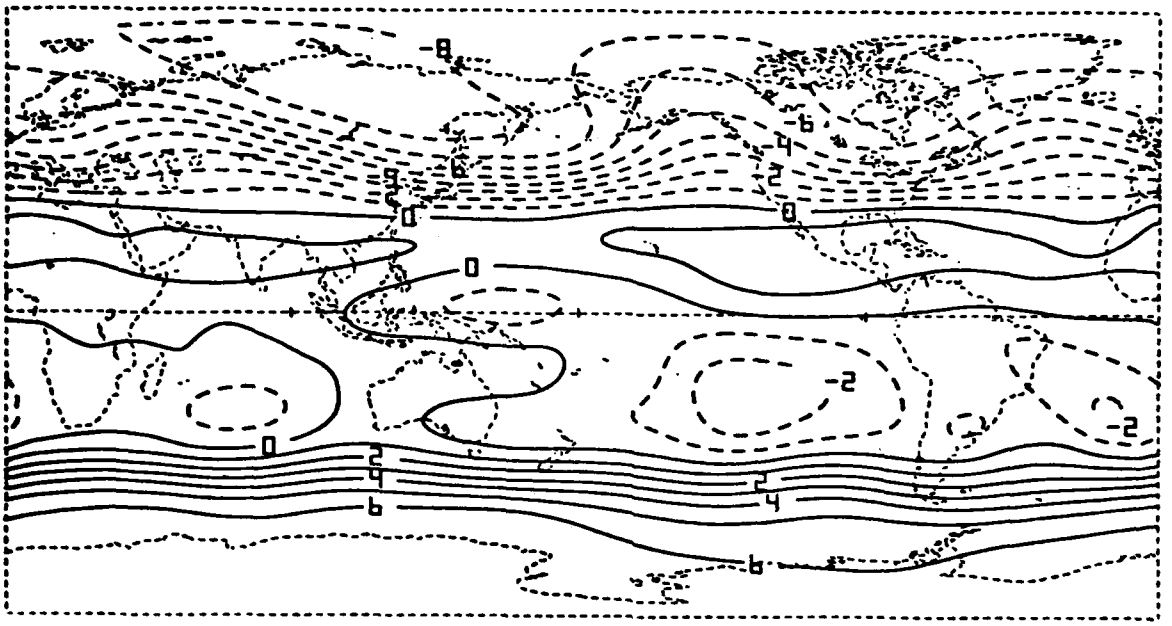

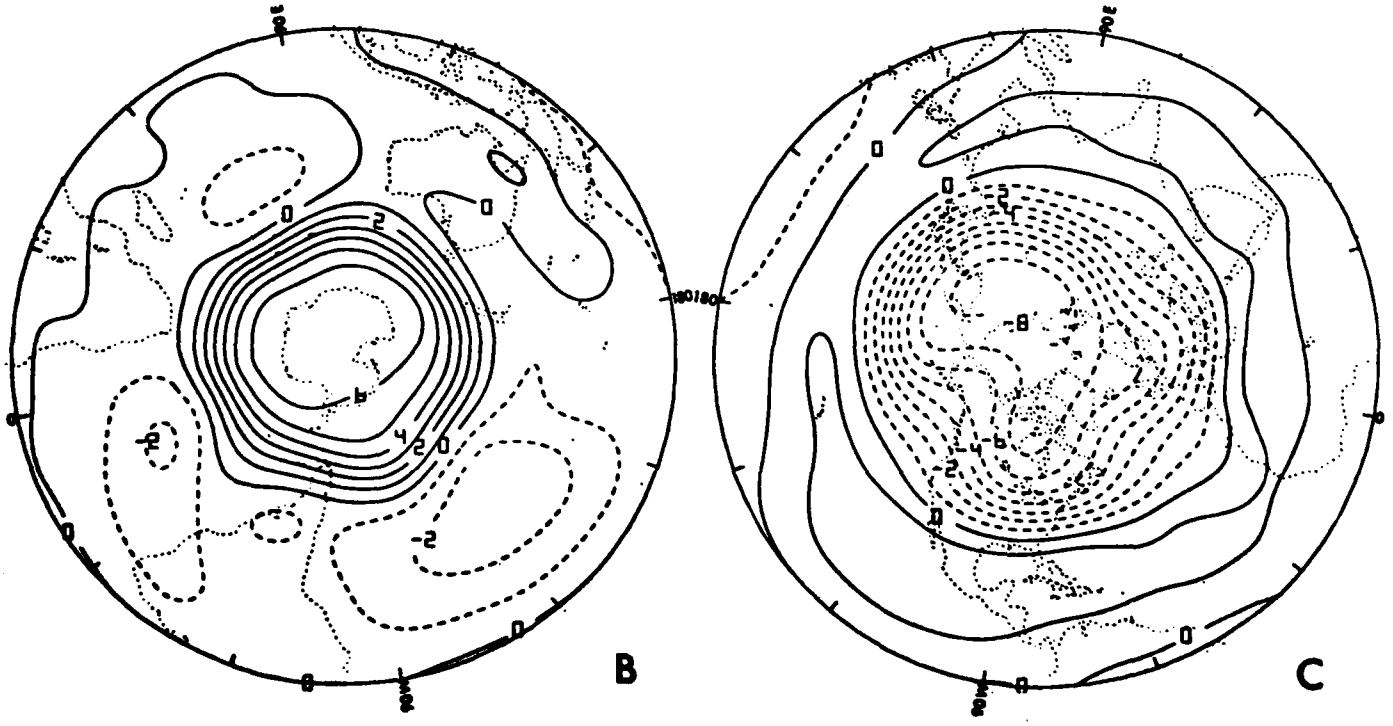

Figure 1. Mass stream function for the 300-310 K isentropic layer of January 1979 on global Mercator (A) and Southern (B) and Northern (C) Hemisphere polar stereographic projections (units, 10^9 kg K^{-1} s^{-1}). Rotational component of isentropic mass transport, $\rho J \underset{\sim}{U}_\psi$, is parallel to the contours with lower values to the left.

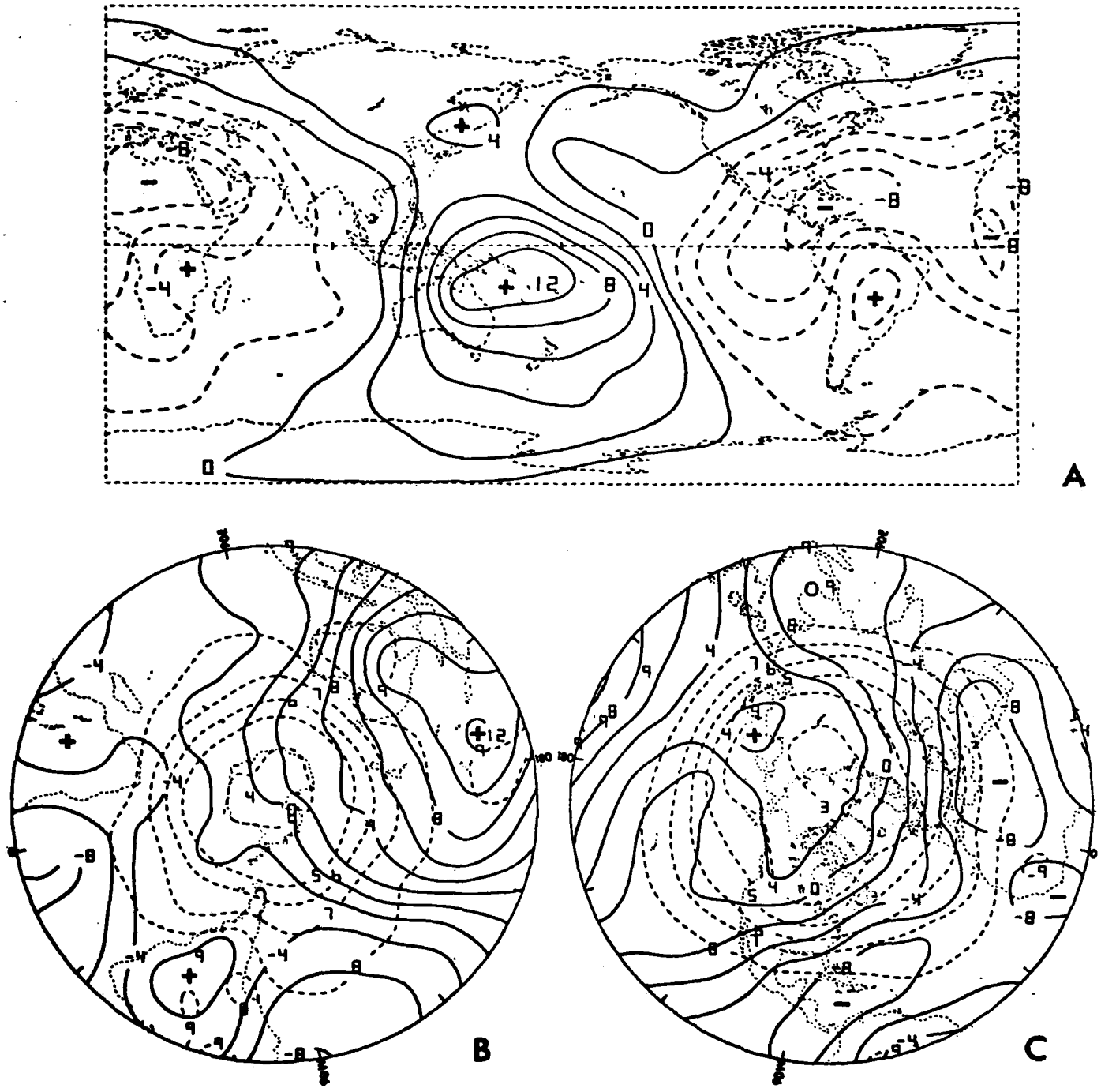

Figure 2. Mass transport potential (solid and dashed lines in (A), solid lines only in (B) and (C)) for the 300-310 K isentropic layer of January 1979 on global Mercator (A) and Southern (B) and Northern (C) Hemisphere polar stereographic projections (units, 10^8 kg K^{-1} s^{-1}). Plus and minus signs indicate relative maxima and minima, respectively, in the potential field. Irrotational component of isentropic mass transport, $\rho J \underline{U}_\chi$, is perpendicular to the contours from lower to higher values. Dashed contours in (B) and (C) represent the mean pressure of the isentropic layer (units, 10^2 mb).

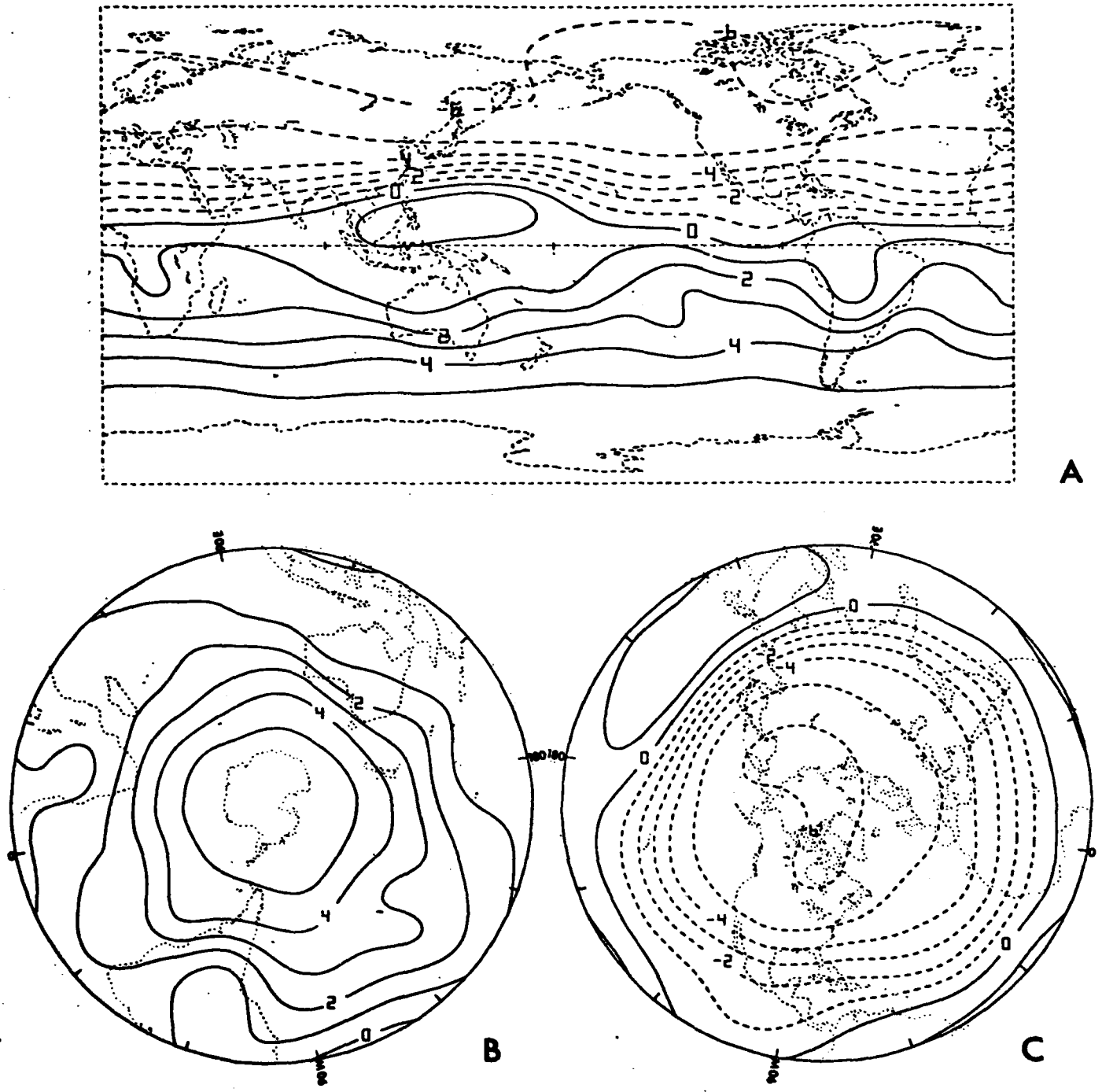

Figure 3. Mass stream function for the 340-350 K isentropic layer of January 1979. Format and legend same as Figure 1.

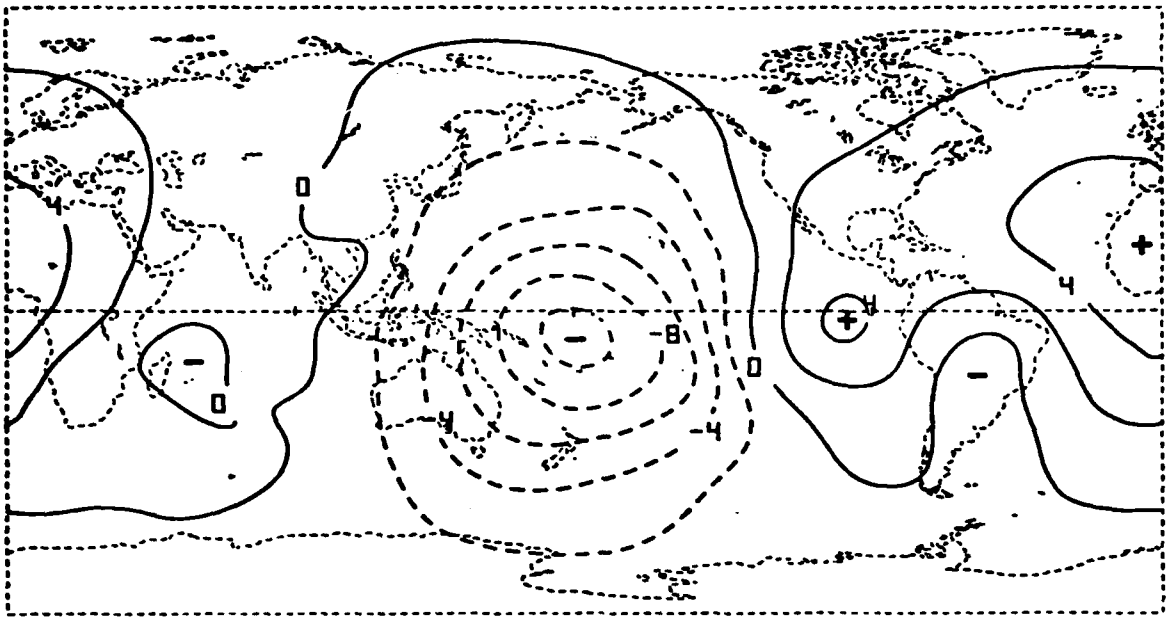

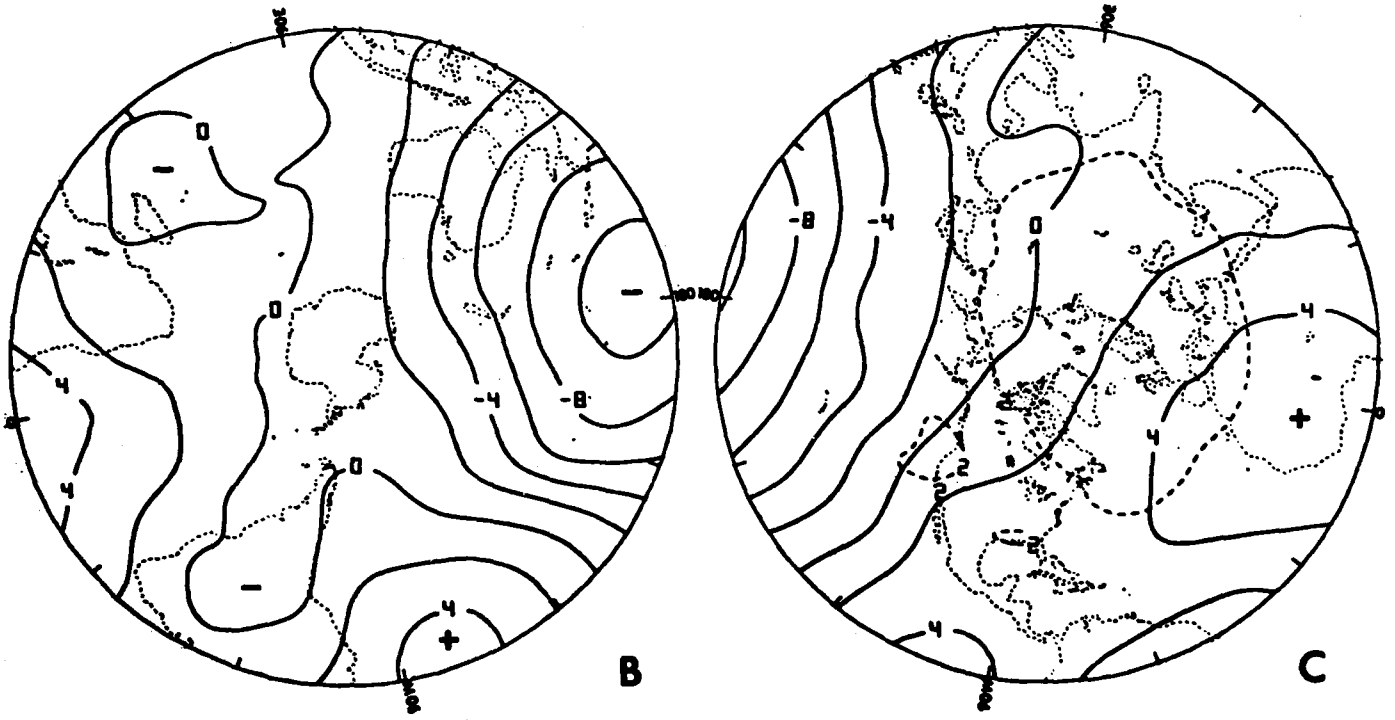

Figure 4. Mass transport potential for the 340-350 K isentropic layer of January 1979. Format and legend same as Figure 2. The mean pressure of the layer is between 300 and 200 mb in B.

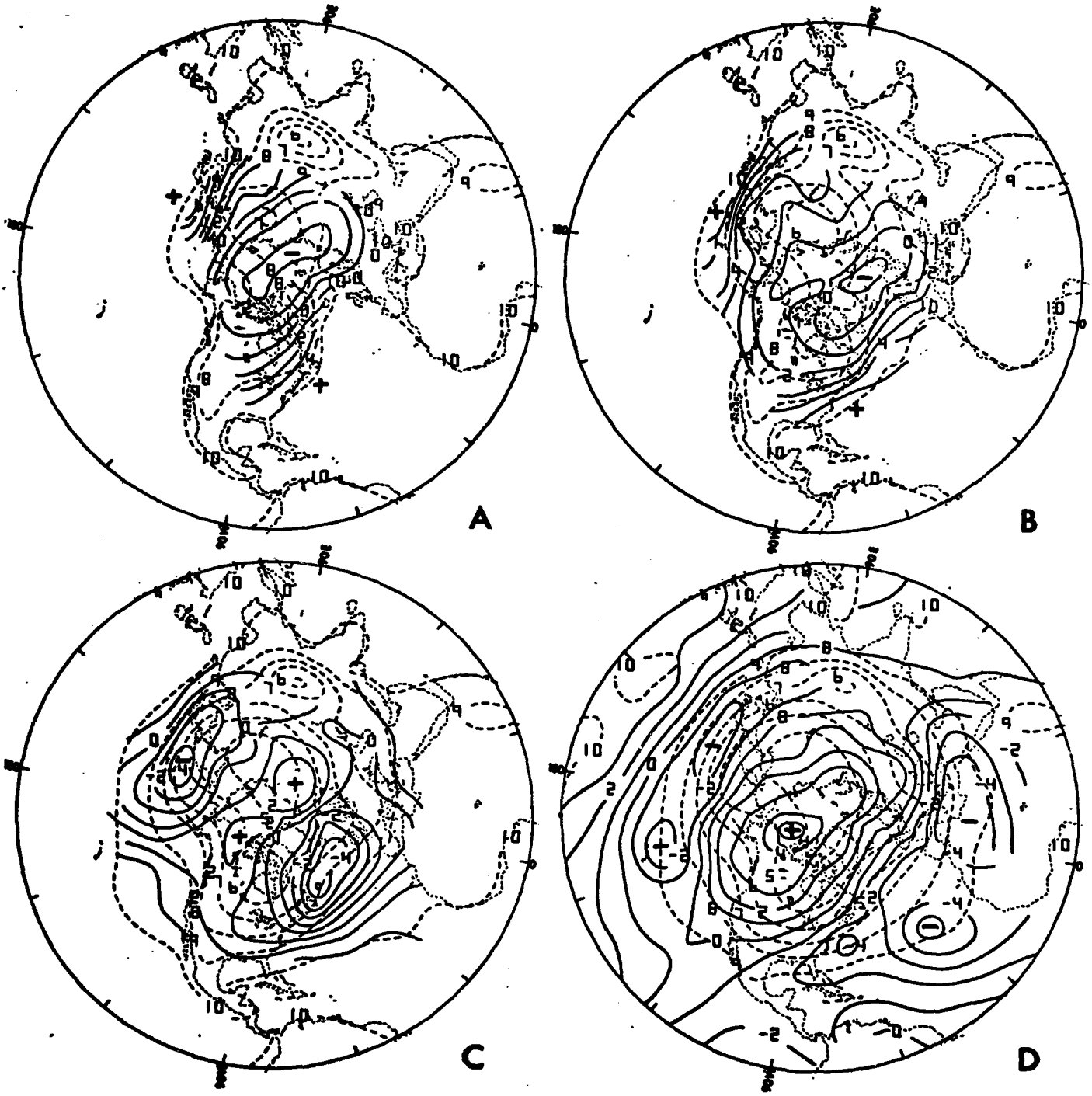

Figure 5. Mass transport potential (solid contours) for 260-270 K (A), 270-280 K (B), 280-290 K (C), and 290-300 K (D) isentropic layers for the Northern Hemisphere of January 1979 (units, 10^8 kg K^{-1} s^{-1}). The potential field is contoured only where the isentropic layer is above the earth's surface. Plus and minus signs indicate relative maxima and minima, respectively, in the potential field. Irrotational component of isentropic mass transport, $\rho J \underset{\sim}{U}_\chi$, is perpendicular to the contours from lower to higher values. Dashed contours represent the mean pressure of the isentropic layer (units, 10^2 mb).

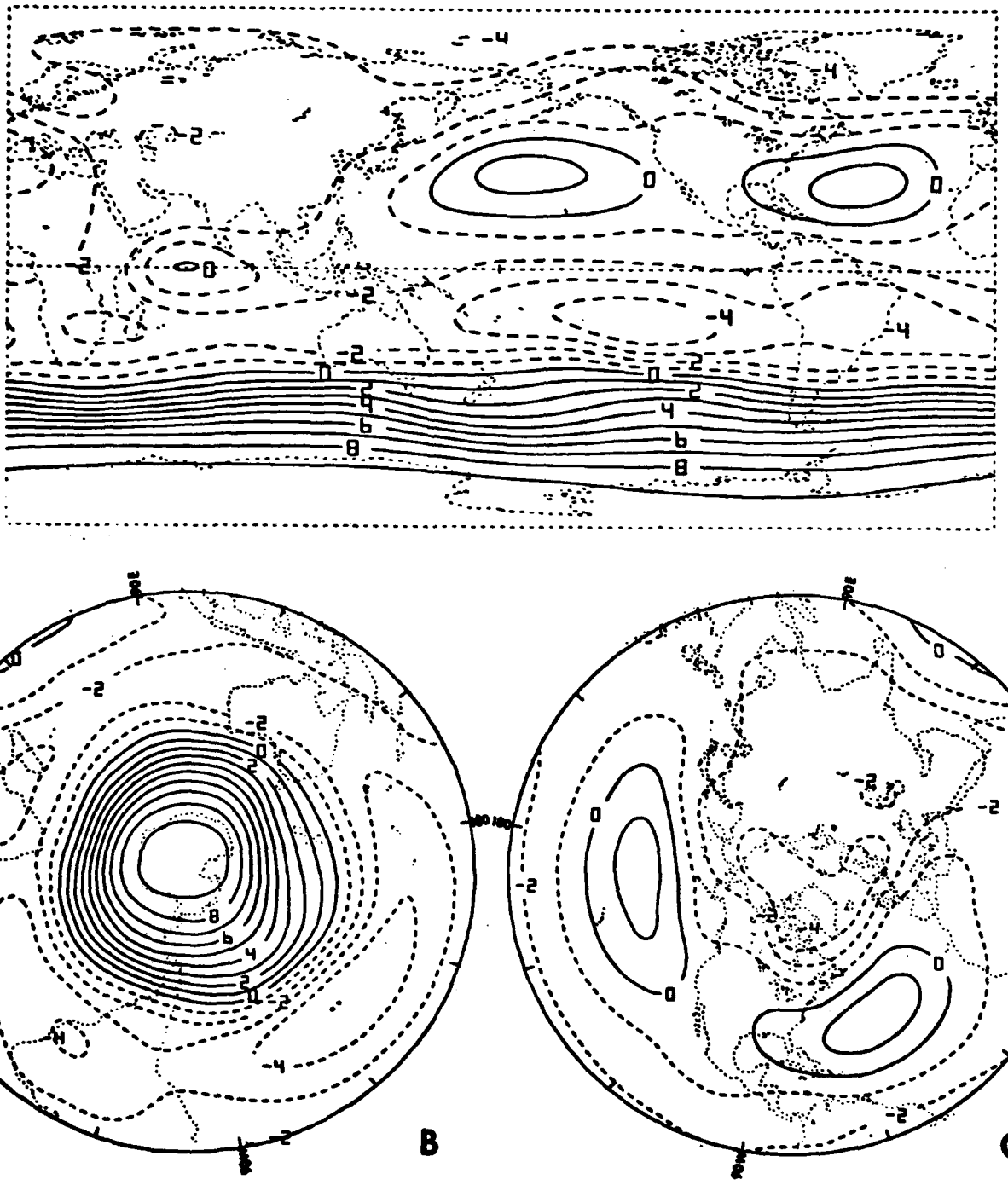

Figure 6. Mass stream function for the 300-310 K isentropic layer of July 1979. Format and legend same as Figure 1.

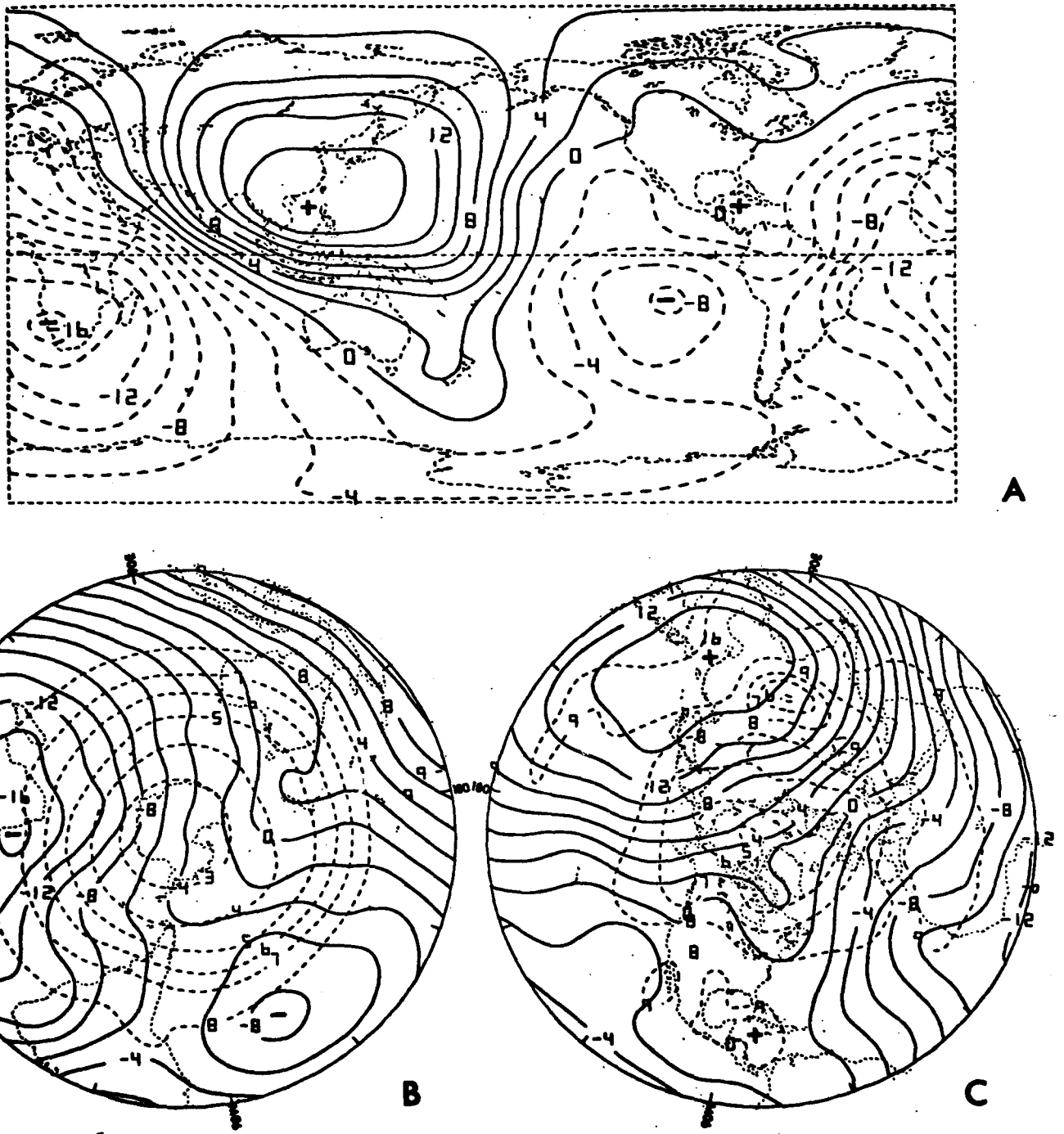

Figure 7. Mass transport potential for the 300-310 K isentropic layer of July 1979. Format and legend same as Figure 2.

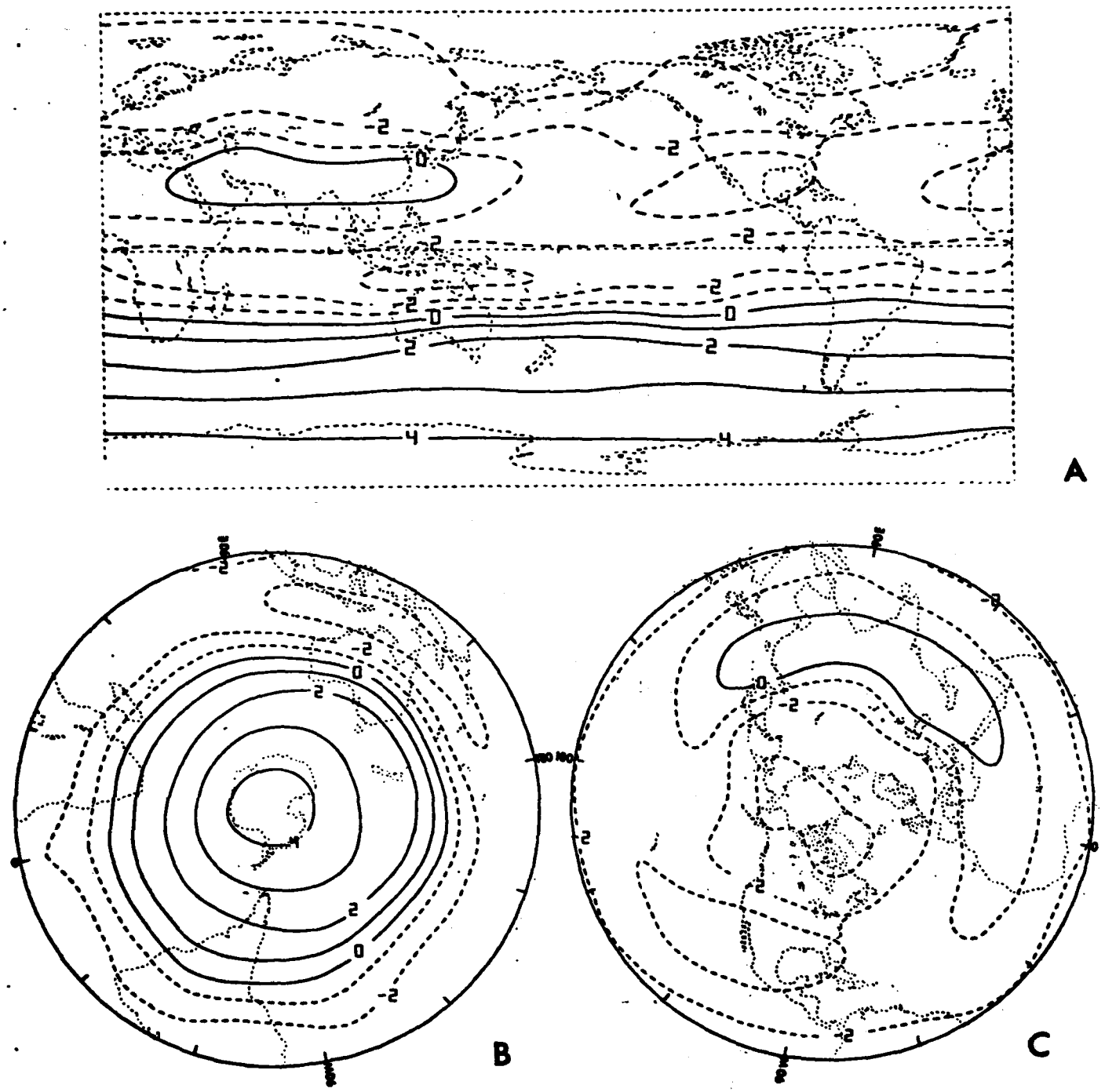

Figure 8. Mass stream function for the 340-350 K isentropic layer of July 1979. Format and legend same as Figure 1.

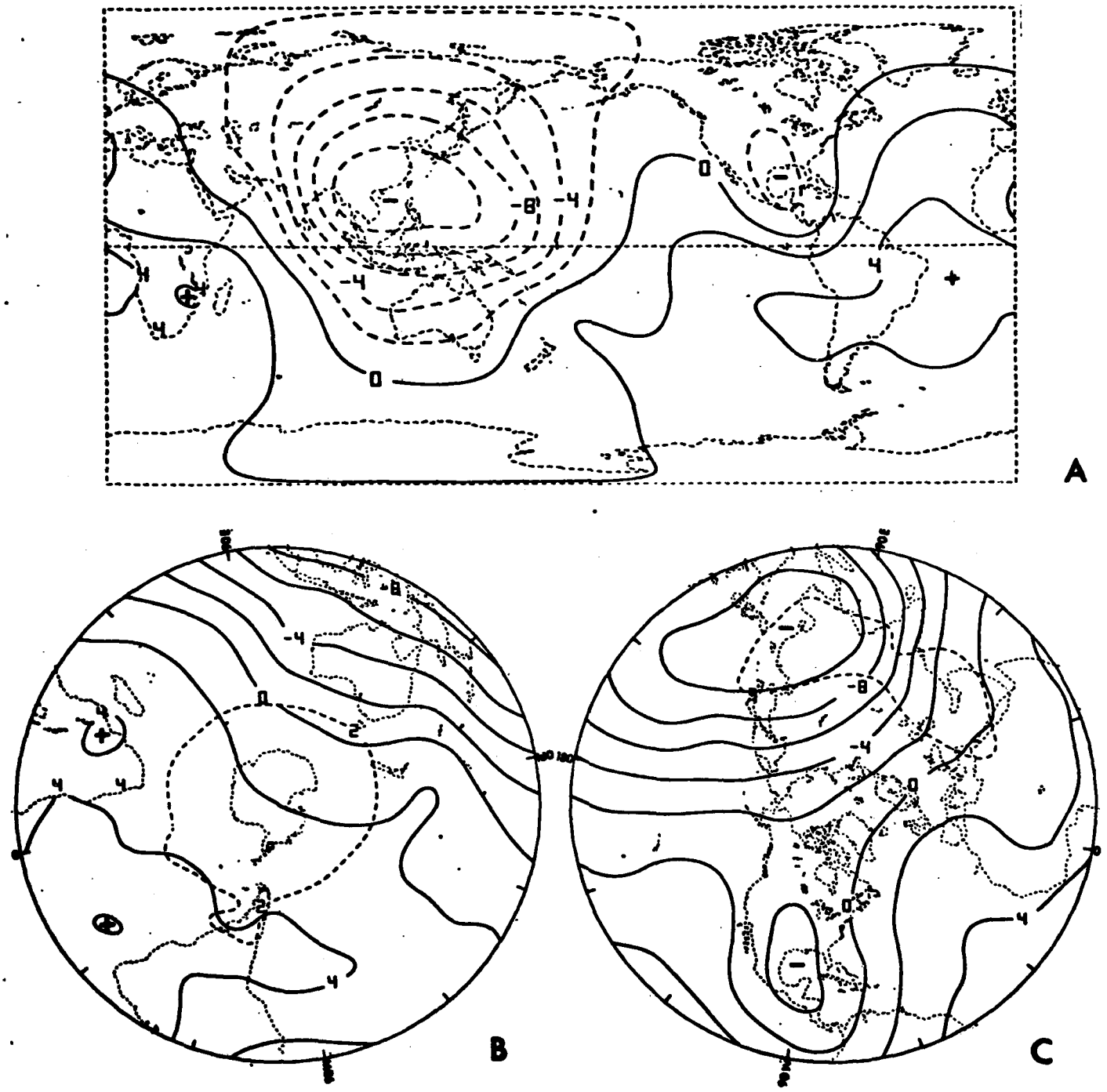

Figure 9. Mass transport potential for the 340-350 K isentropic layer of July 1979. Format and legend same as Figure 2.

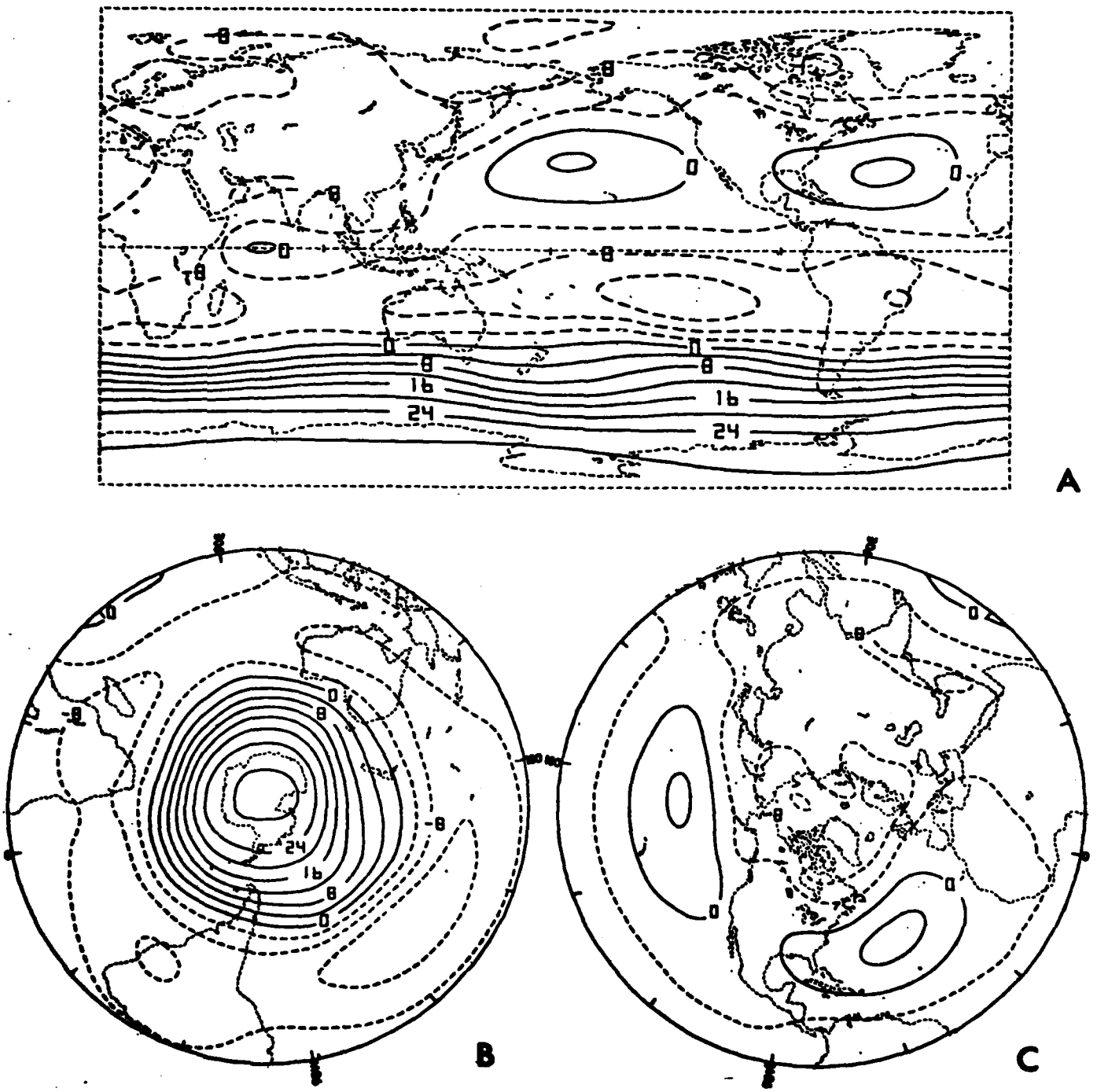

Figure 10. Energy stream function for the 300-310 K isentropic layer of July 1979 on global Mercator (A) and Southern (B) and Northern (C) Hemisphere polar stereographic projections (units, 10^{14} J K^{-1} s^{-1}). Rotational component of isentropic energy transport, $\rho J \underline{v}_\psi$, is parallel to the contours with lower values to the left.

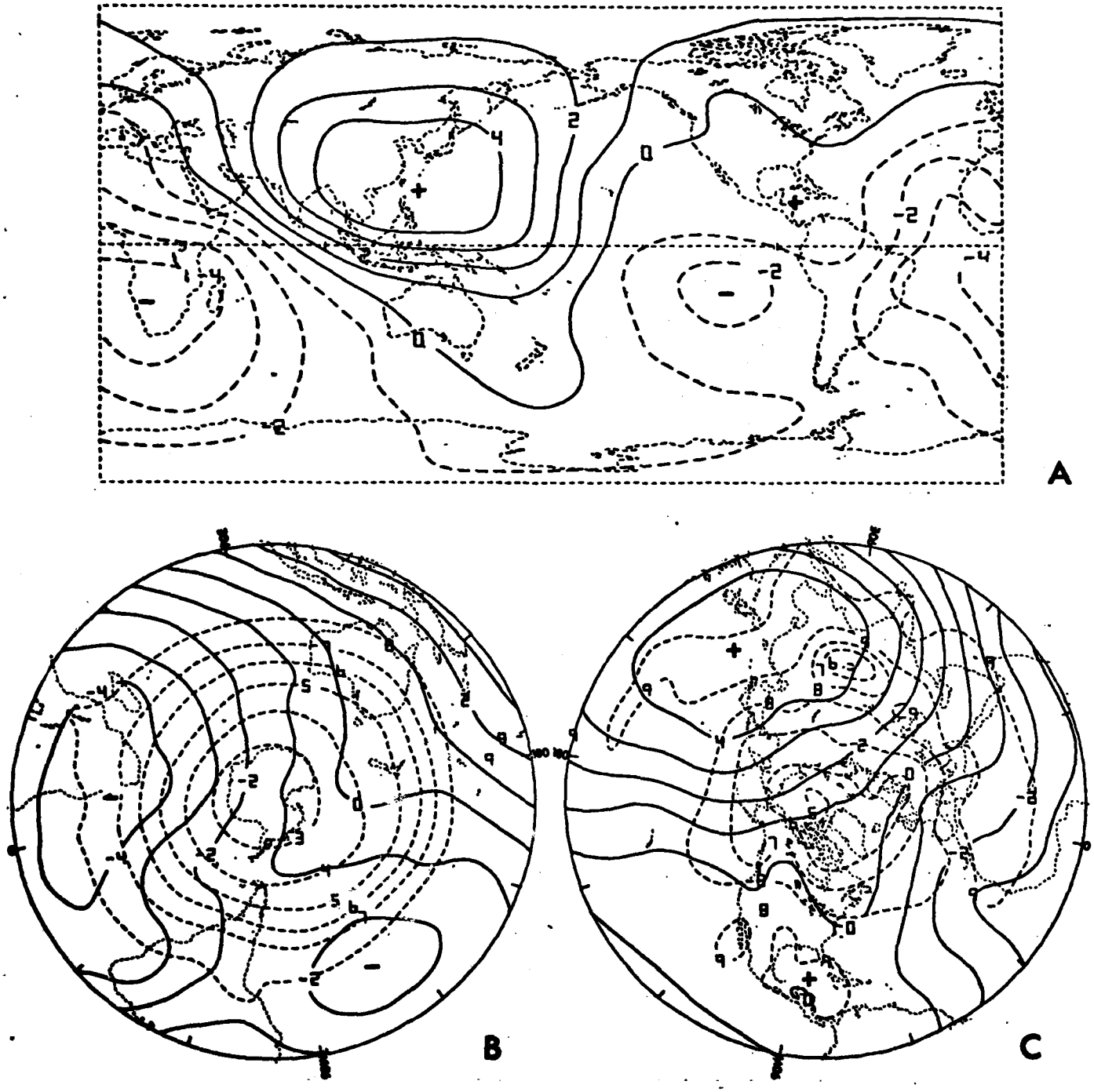

Figure 11. Energy transport potential (solid and dashed lines in (A), solid lines only in (B) and (C)) for the 300-310 K isentropic layer of July 1979 on global Mercator (A) and Southern (B) and Northern (C) Hemisphere polar stereographic projections (units, 10^{14} J K^{-1} s^{-1}). Plus and minus signs indicate relative maxima and minima, respectively, in the potential field. Irrotational component of isentropic energy transport, $\rho J \underline{U} v_\chi$, is perpendicular to the contours from lower to higher values. Dashed contours in (B) and (C) represent the mean pressure of the isentropic layer (units, 10^2 mb).

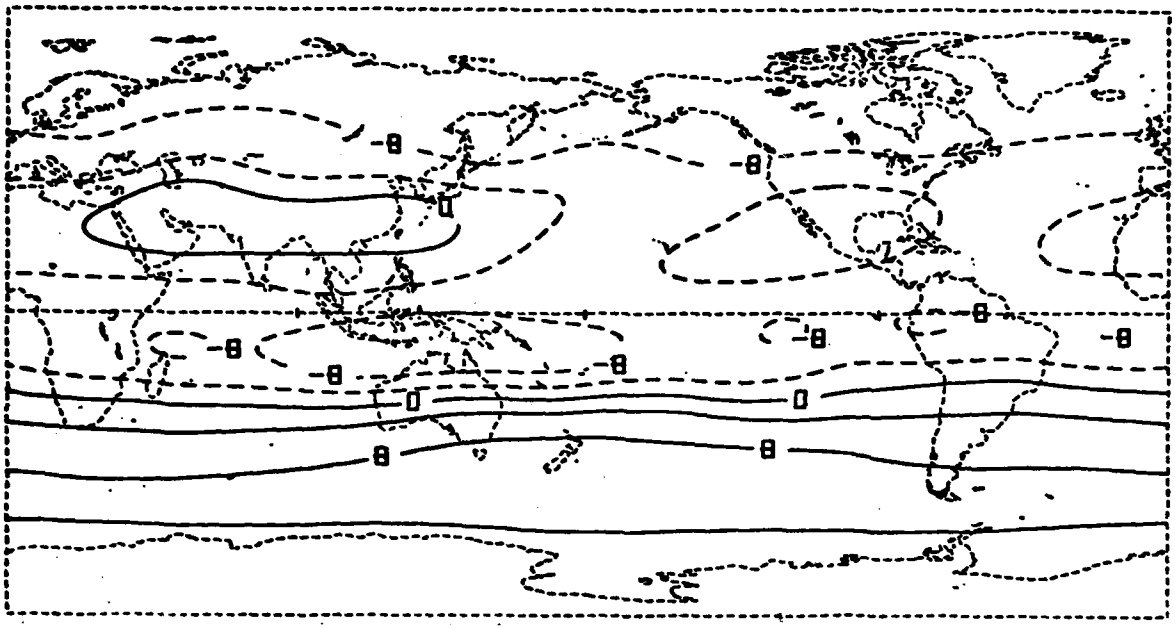

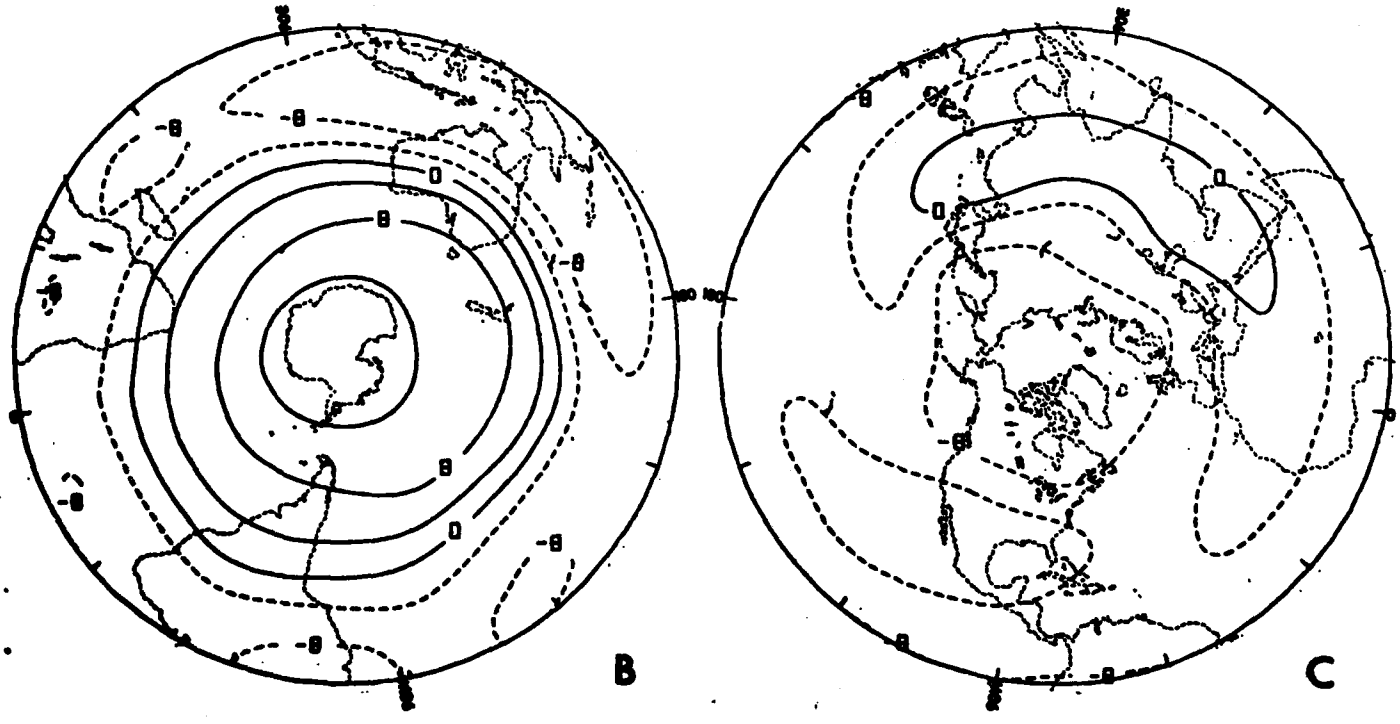

Figure 12. Energy stream function for the 340-350 K isentropic layer of July 1979. Format and legend same as Figure 10.

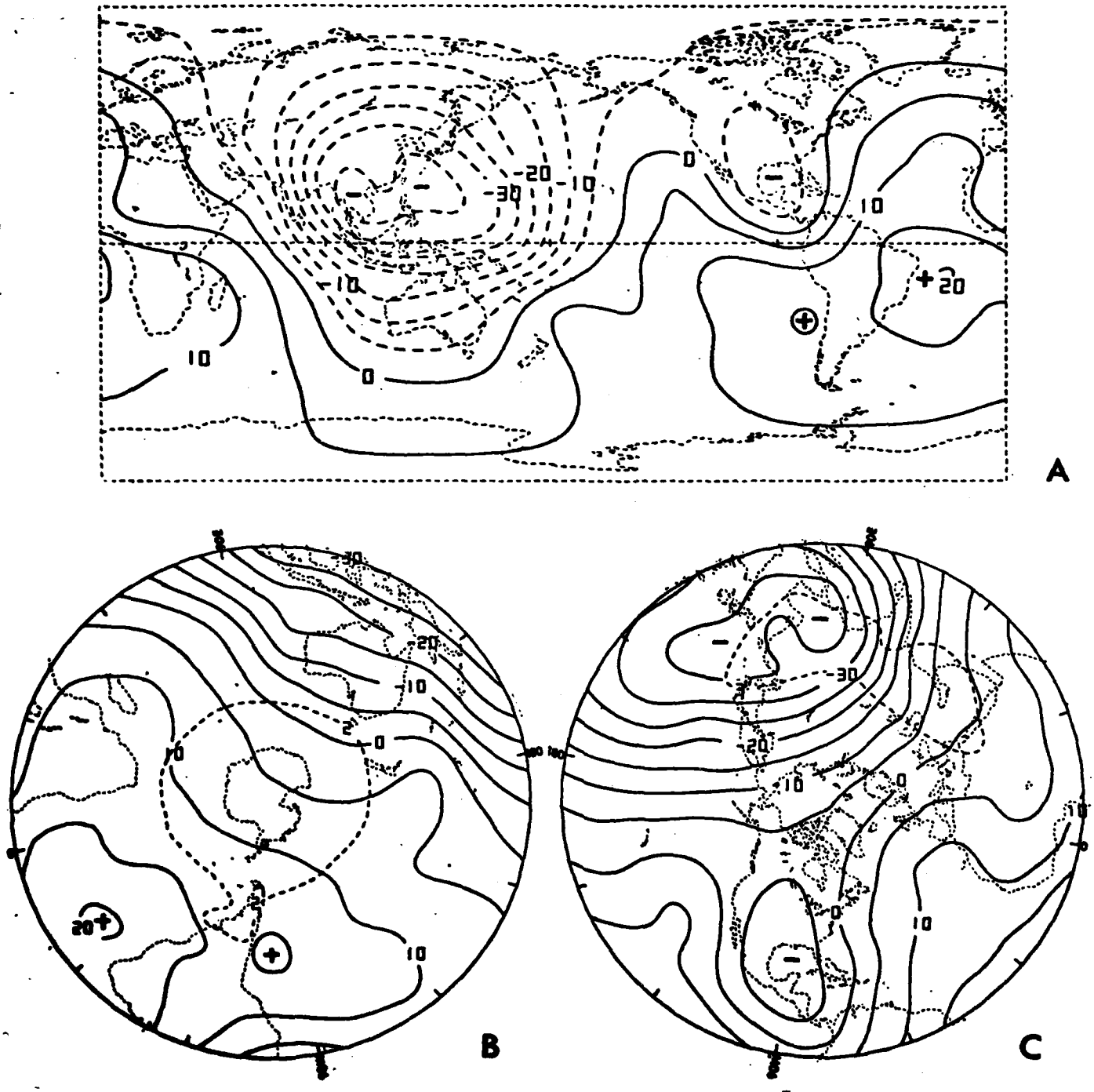

Figure 13. Energy transport potential for the 340-350 K isentropic layer of July 1979. Format and legend same as Figure 11 except potential units are 10^{13} J K^{-1} s^{-1}.

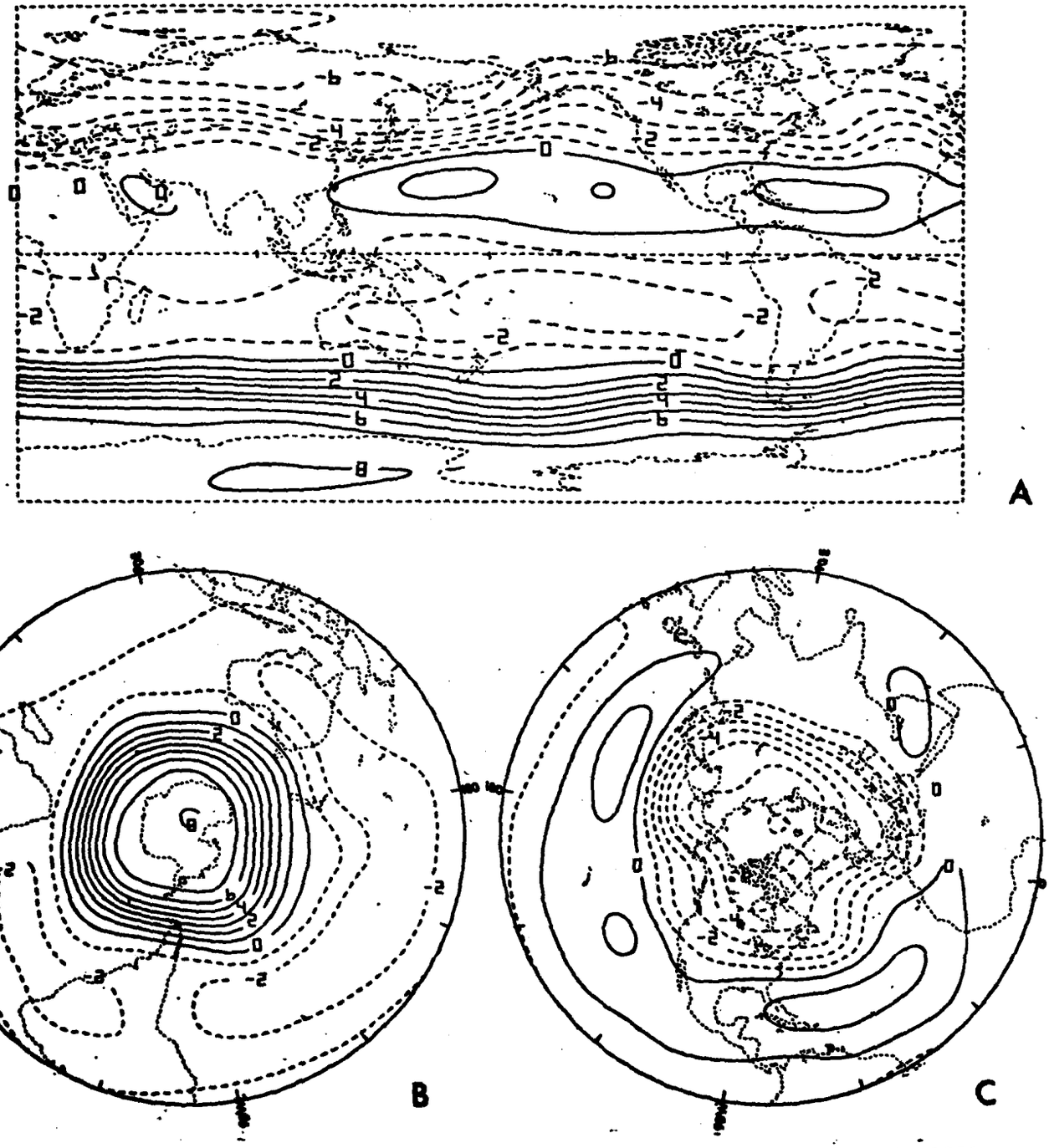

Figure 14. Mass stream function for the 300-310 K isentropic layer of April 1979. Format and legend same as Figure 1.

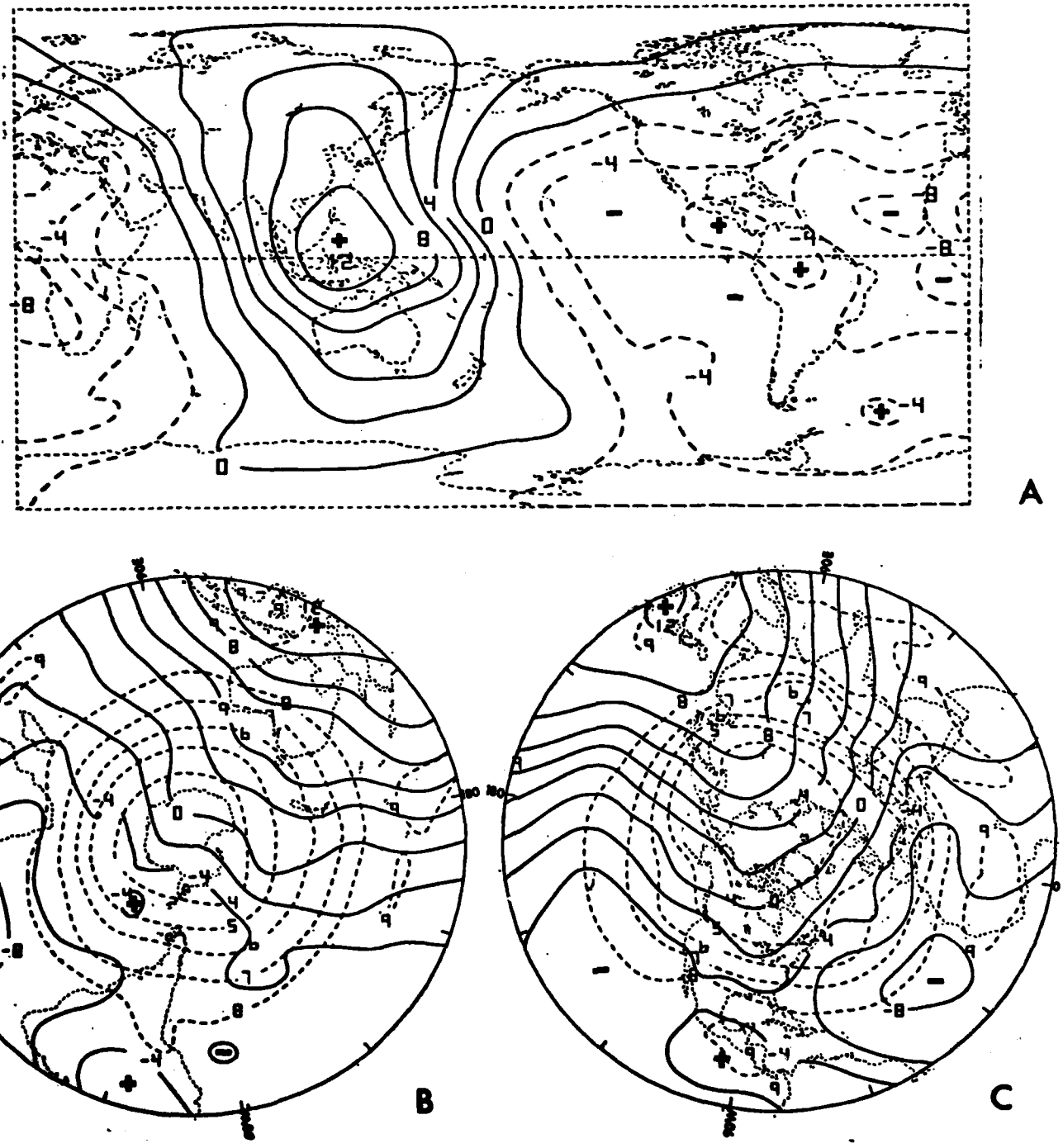

Figure 15. Mass transport potential for the 300-310 K isentropic layer of April 1979. Format and legend same as Figure 2.

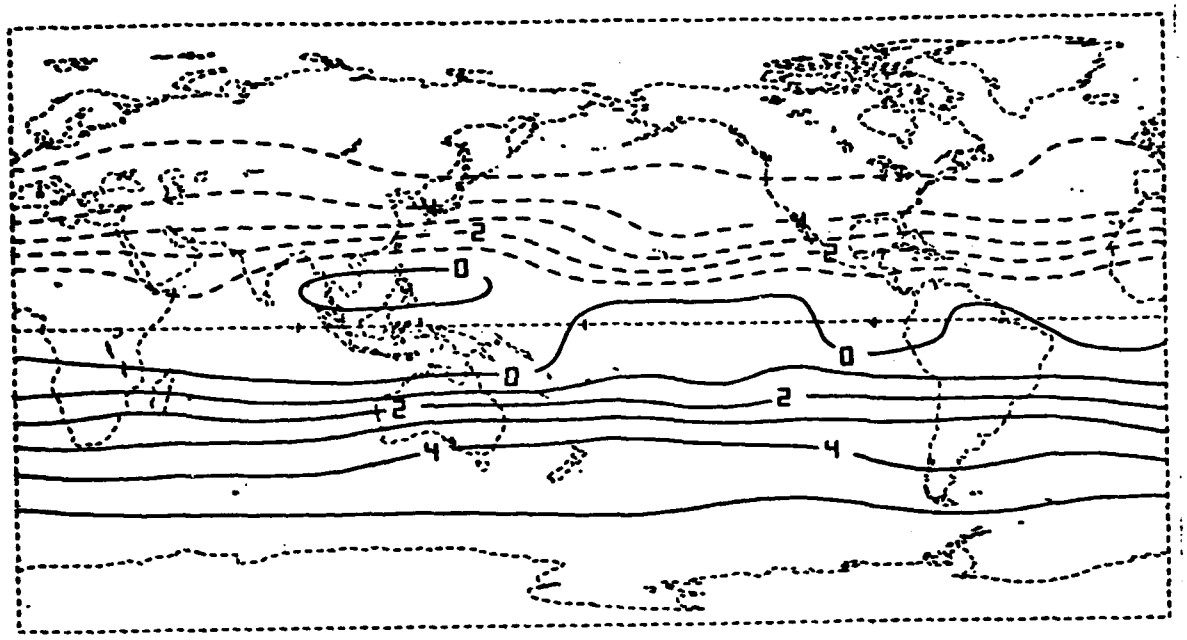

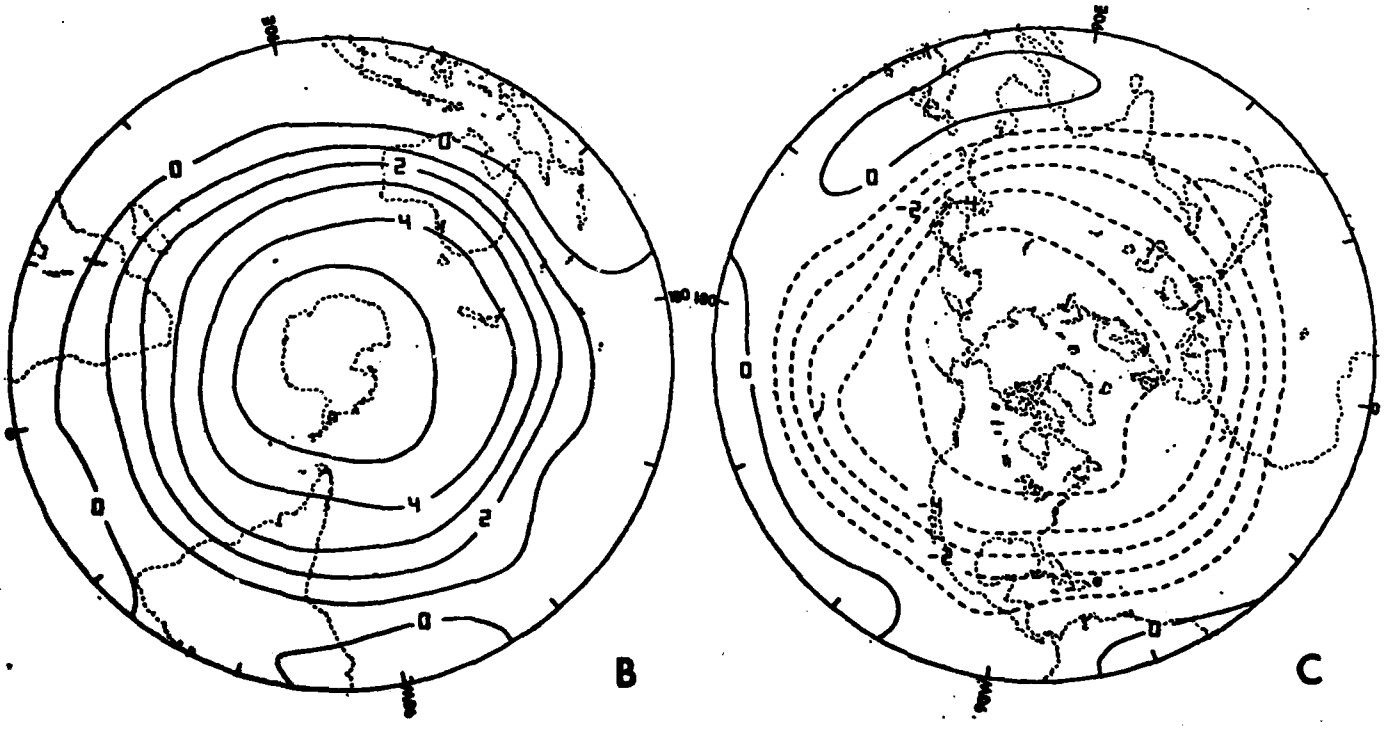

Figure 16. *Mass stream* **function for the 340-350 K isentropic layer of April 1979. Format and legend same as Figure 1.**

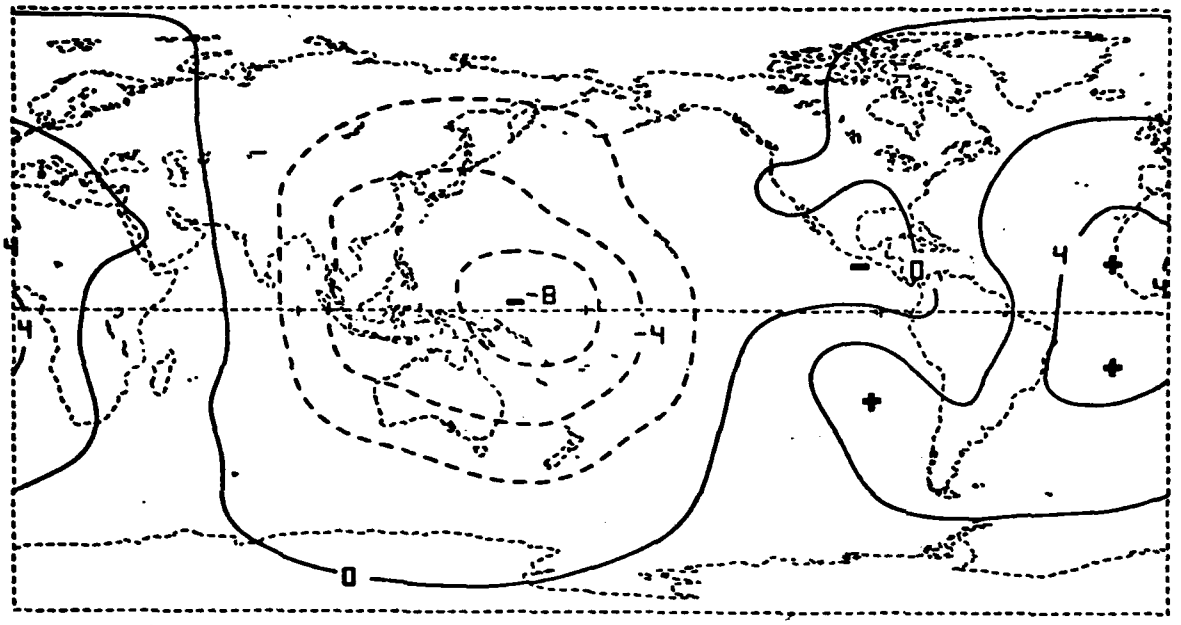

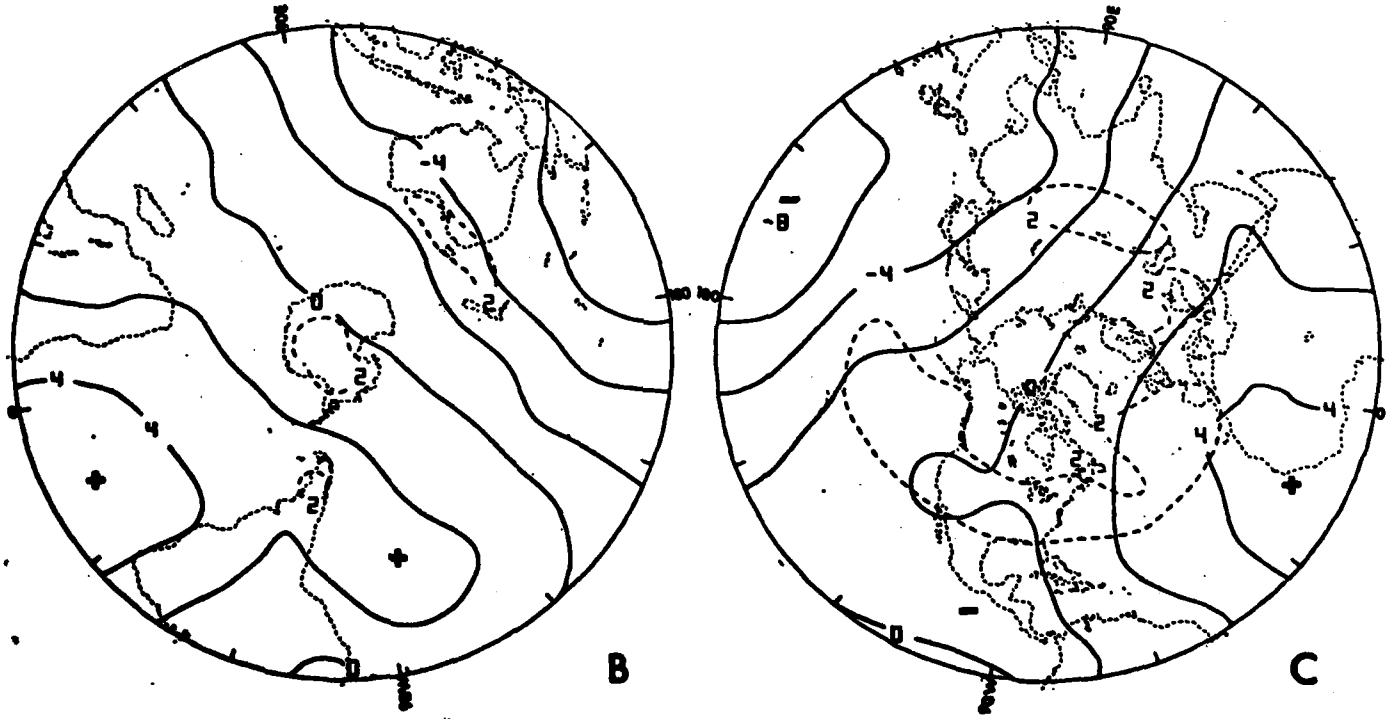

Figure 17. Mass transport potential for the 340-350 K isentropic layer of April 1979. Format and legend same as Figure 2.

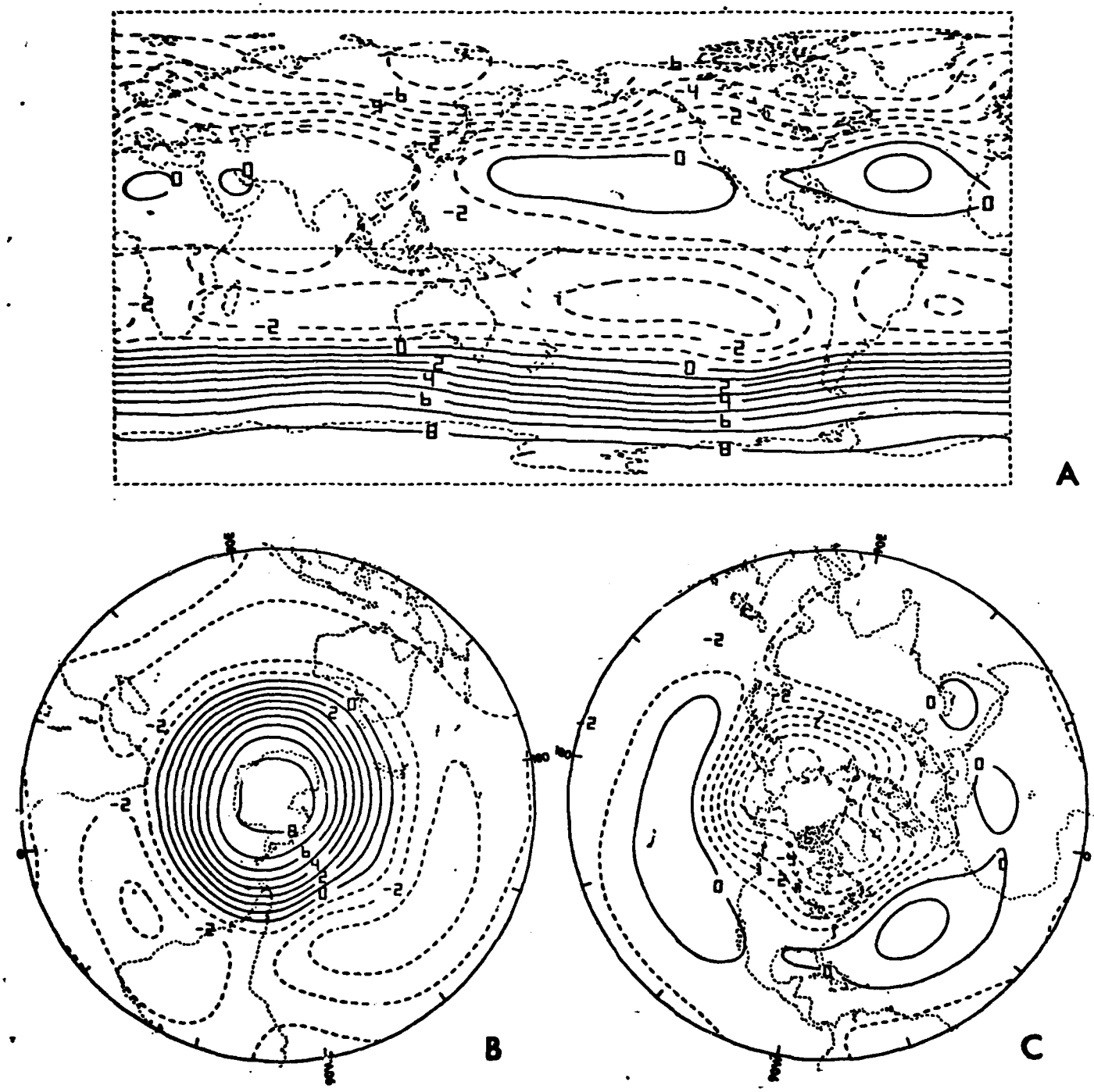

Figure 18. Mass stream function for the 300-310 K isentropic layer of October 1979. Format and legend same as Figure 1.

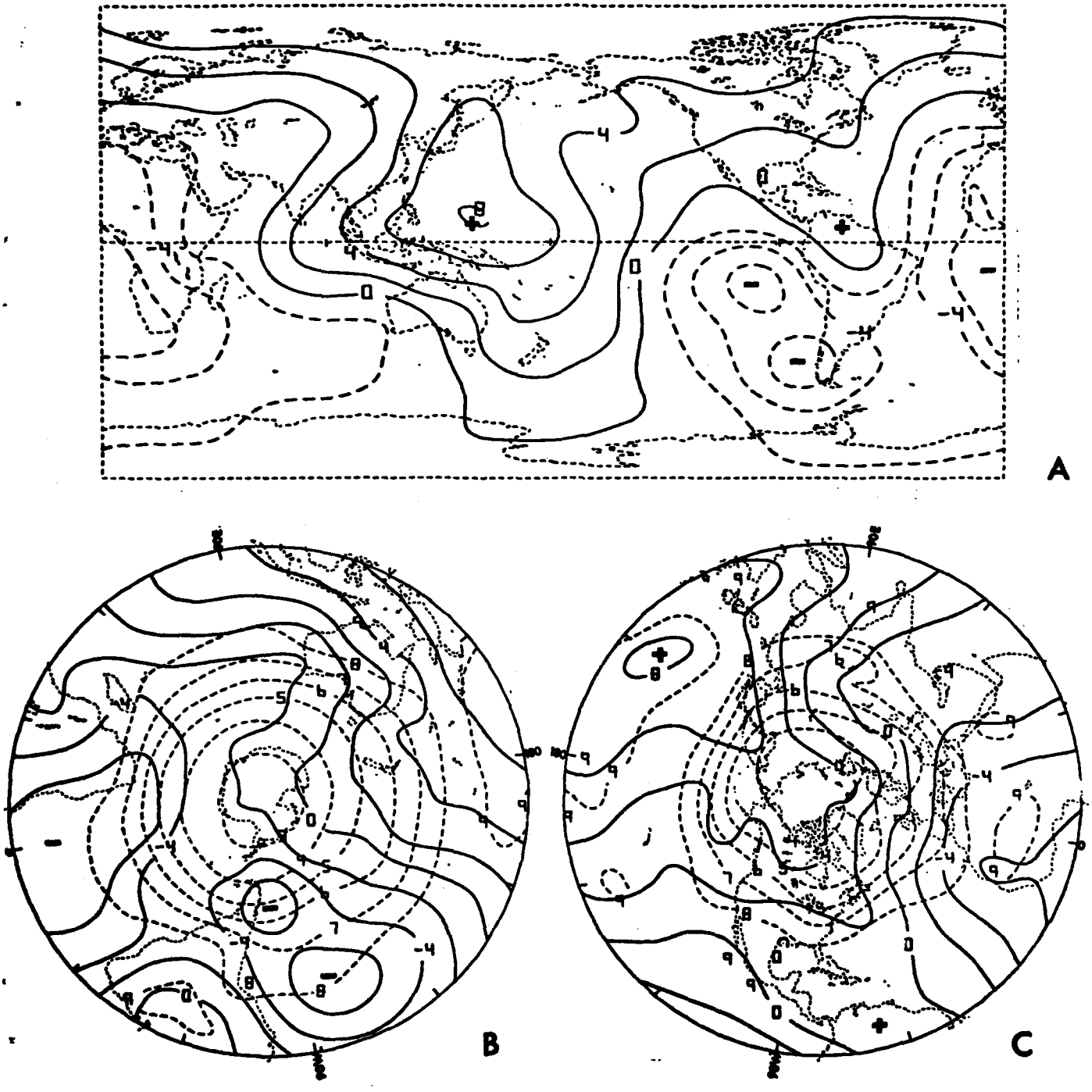

Figure 19. Mass transport potential for the 300-310 K isentropic layer of October 1979. Format and legend same as Figure 2.

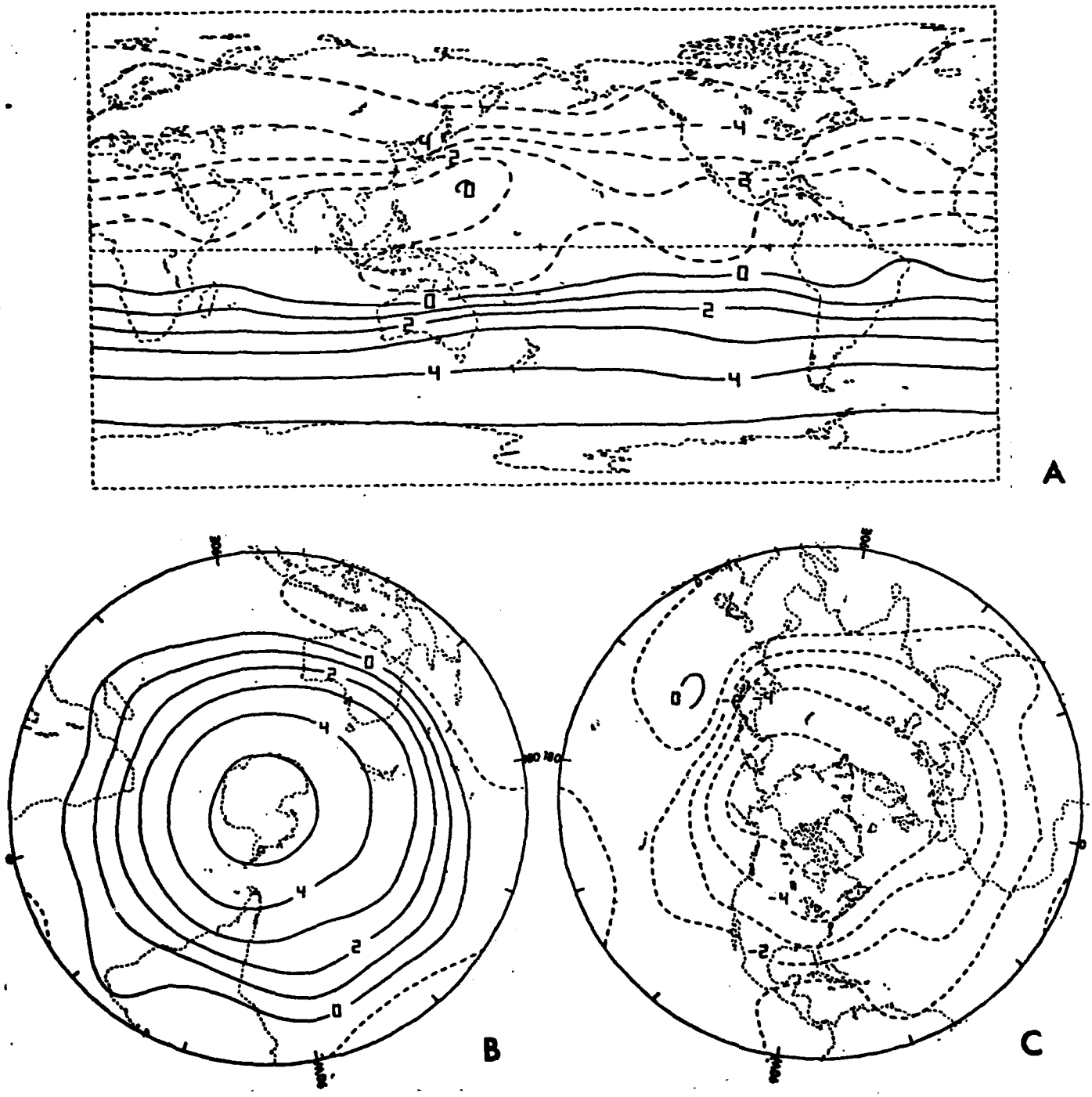

Figure 20. Mass stream function for the 340-350 K isentropic layer of October 1979. Format and legend same as Figure 1.

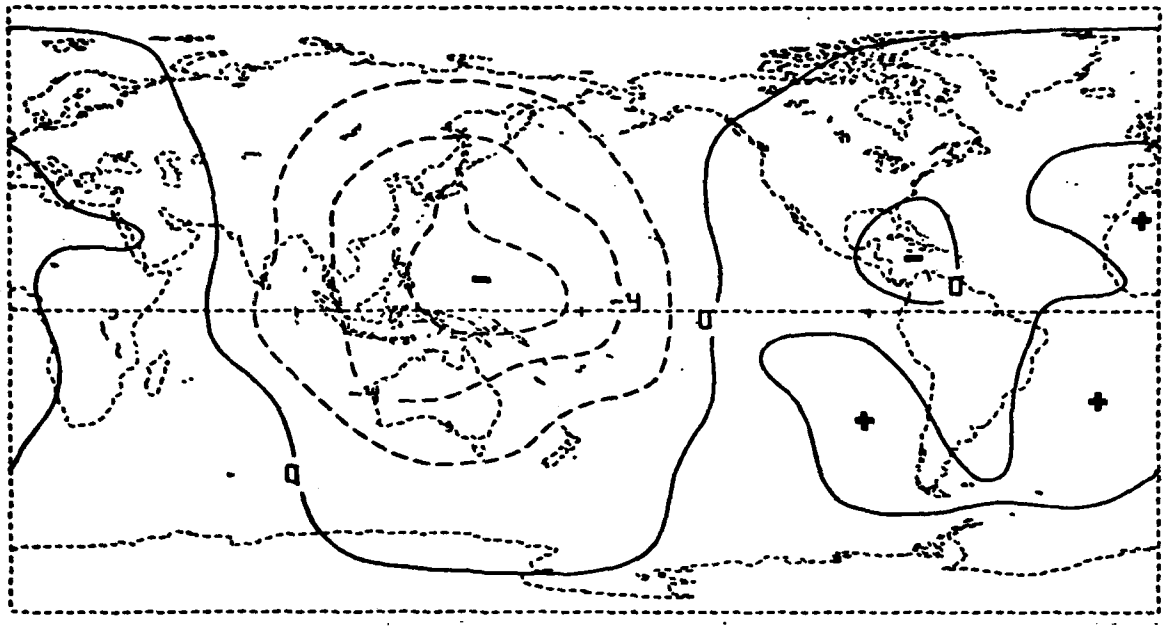

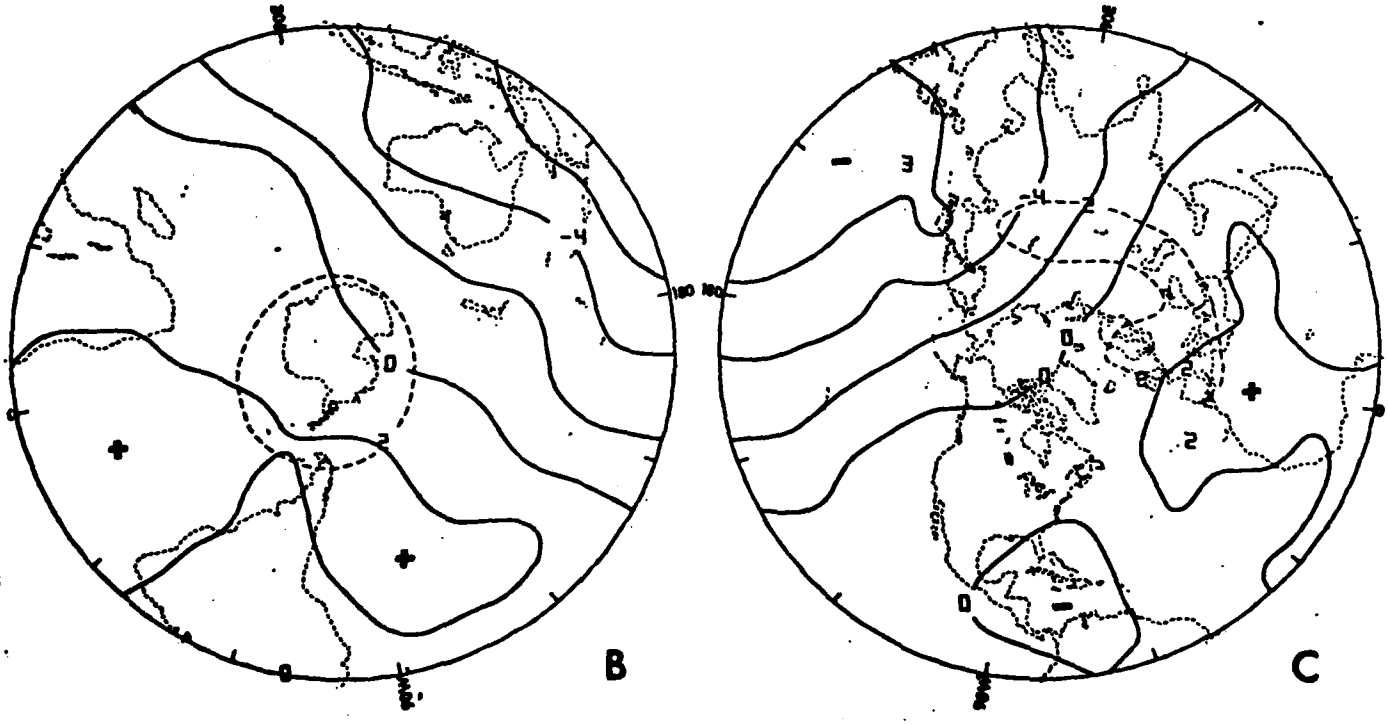

Figure 21. Mass transport potential for the 340-350 K isentropic layer of October 1979. Format and legend same as Figure 2.


MED
8